2004

ANNUAL REPORT
FUSION RESEARCH CENTER
GEORGIA INSTITUTE OF TECHNOLOGY
ATLANTA, GA 30332

W. M. STACEY

J. MANDREKAS

OCTOBER, 2004

Collaborators:

Georgia Tech Faculty W. J. Lackey (ME), C. de Oliveira (NRE), D. W. Tedder (ChBE)

Georgia Tech NRE Students V. L. Beavers, W. A. Casino, J. R. Cheatham, L. A. Cottrill, Z. W.Friis, R. D. Green, G. C. Hahn, W. R. Hamilton, K. W. Haufler, J. D. Hutchinson, G. P. Kessler, C. M. Kirby, R. A. Lorio, J. W. Maddox, A. A. Manzoor, A. N. Mauer, J. J. Noble, C. A. Noelke, D. M. Stopp, M. Park, M. R. Terry, D. S. Ulevich, D-K. Zhang

Argonne National Laboratory, Nuclear Engineering Div. E. A. Hoffman

General Atomics, Fusion Division R. J. Groebner, A. W. Leonard, T. W. Petrie, P. H. West

Oak Ridge National Laboratory, Fusion Division R. J. Colchin, L. W. Owen, M. Murakami

Lawrence Livermore National Laboratory M.V. Umansky

I. COLLABORATIVE ANALYSIS OF DIII-D (DoE Grant ER54538)

A. SUMMARY

The collaboration of the Georgia Tech Fusion Research Center in the analysis and interpretation of DIII-D experiments as part of the national DIII-D Team began in 1998 under support from General Atomics and has continued since 1999 under support of DoE OFES (Grant DE-FG02-ER54538). This analysis and interpretation of DIII-D experiments has been closely integrated with the ongoing, internally supported code and theory development in the Georgia Tech Fusion Research Center, and results of both efforts are discussed in this section without distinction. The principal areas of experimental analysis and interpretation have been: 1) the physics of the edge pedestal; 2) density limits caused by thermal instabilities in the plasma edge; 3) plasma rotation; 4) neutral atom fueling and recycling in the plasma edge; and 5) impurity transport in general and the radiating mantle in particular.

B. PHYSICS OF THE EDGE PEDESTAL

1. Background

The 'pedestal' structure of the density and temperature profiles in the edge of H-mode plasmas has been the subject of intensive research for a number of years (see Ref. 1 for review). This interest is motivated in part by the recognition that core transport calculations of the performance of future fusion reactors depend sensitively on the value of the pedestal density and, in particular, the pedestal temperature used as boundary conditions in these calculations[2,3].

Many pedestal investigations have focused on understanding the magnetohydrodynamic (MHD) instabilities that limit the pressure or pressure gradient in the edge pedestal (e.g. Refs. 4-9) or on identifying the experimental relations among MHD instability parameters, device operating parameters, and pedestal parameters (e.g. Refs. 10-13). Correlations of measured pedestal density and temperature values and pedestal profile widths with various MHD and plasma operating parameters have led to theory-based empirical scaling laws (e.g. Ref. 14).

While the MHD instabilities that limit the edge pressure and pressure gradients have been the subject of the majority of the investigations to date, there also have been both i) studies of transport (e.g Refs 15 and 16) and other (e.g Refs.17-19) mechanisms that could cause the formation of the H-mode pedestal and ii) studies of the causes of the observed pedestal structure--widths and gradients of the density and temperature profiles—(e.g. Refs. 20-28). The importance of the ionization of recycling neutrals and of the formation of a negative radial electric field well in determining the edge pedestal structure have been suggested by several of these authors. We note that while the pedestal is modeled

presently in many sophisticated edge and core plasma calculations (e.g. Refs. 29-31) by adjusting transport coefficients in the particle and energy balance equations to obtain agreement with experimental profiles, we are here proposing fundamental studies to determine the causes of the pedestal structure.

2. Work on Edge Pedestal under Grant ER54538

A theoretical model for the density and temperature gradients and widths in the edge pedestal was developed in a series of papers[32-34] from considerations of the MHD stability constraints on the pressure/pressure gradient, of the transport constraints on the temperature and density gradients, and of the observed similarity between the density width and the neutral penetration mean-free-path. This model was tested against DIII-D data[35] and a rough agreement of prediction with experiment was found, but the lack of knowledge of transport coefficients in the edge pedestal and the unavailability of a usable characterization of the MHD stability surface in terms of the edge parameters were identified as impediments to the development of a fully predictive analytical edge pedestal model.

This situation led to an investigation of transport phenomena in the DIII-D edge pedestal[36]. A comparison of various heat conduction theories with data from several DIII-D shots indicated: 1) that neoclassical theory is in somewhat better agreement with experiment than is ITG theory for the ion thermal conductivity, although both agree reasonably well with the thermal conductivity values inferred from the data; 2) that ETG theory ($k_\perp c_s \leq \omega_e$) is in much better agreement with experiment than is electron drift wave theory ($k_\perp c_s \leq \Omega_i$) for the electron thermal conductivity. New theoretical expressions were found for a "diffusive-pinch" particle flux, for the inference of the radial momentum transfer frequency in the edge, and for the density gradient scale length. It was found that neither atomic physics nor convection could account for the inferred momentum transfer rates in the edge, but that gyroviscosity was the right order of magnitude.

The theoretical development of particle transport in the plasma edge directly from the particle and momentum balance equations was extended in a series of papers[37-39] and applied to interpret DIII-D edge pedestal measurements[40]. The resulting calculation model is as follows. The particle and heat balance equations are numerically integrated inward from the separatrix, using separatrix boundary conditions determined from overall energy and particle balances on the plasma within the separatrix, to obtain profiles of the heat (Q) and particle (Γ) fluxes in the plasma edge. The neutral densities needed to evaluate the atomic physics particle sources and heat losses are calculated with a 2D transport model. The heat conduction relations for ions and electrons, $q = (Q-2.5\Gamma T) = nT\chi L_T^{-1}$, are used to determine the radial profile of L_T^{-1} and then the definitions $-(dT/dr)/T = L_T^{-1} = (Q-2.5\Gamma T)/nT\chi$ are integrated radially inward from the separatrix, using experimental separatrix temperature boundary conditions, to calculate

the ion and electron temperature profiles. The heat conductivities inferred from experiment are used to evaluate these expressions.

The momentum balance equations are solved for the requirement $L_p^{-1} = -(dp/dr)/p = (\upsilon_r - \upsilon_{pinch})/D$, where υ_{pinch} denotes a collection of terms involving the radial electric field (E_r), the toroidal and poloidal rotation velocities (υ_φ and υ_θ), the frequency (ν_d*) for the radial transfer of toroidal momentum, and the toroidal components of the beam momentum input and the induced electric field. The radial electric field and the carbon toroidal and poloidal rotation velocities used in the evaluation of υ_{pinch} are taken from experiment. The quantity D denotes another collection of terms arising, as υ_{pinch} does, from the derivation of the relation for L_p^{-1} from momentum balance. The ion density profile is calculated by numerically integrating $-(dn/dr)/n = L_n^{-1} = L_{pi}^{-1} - L_{Ti}^{-1} = (\upsilon_r - \upsilon_{pinch})/D$ inward from the separatrix, using an experimental separatrix density boundary condition.

This coupled nonlinear set of differential equations is iterated to obtain a converged solution for the radial profiles of density, ion and electron temperatures, particle and heat fluxes, and neutral density in the edge plasma. Thus, these profiles are the consequence of 'classical' particle, momentum and energy balance and the heat conduction relation in the presence of recycling neutrals, given the boundary conditions, transport coefficients and radial electric field and the carbon toroidal and poloidal rotation velocities inferred or taken from experiment. Comparison of these profiles with the directly measured experimental density and temperature profiles thus provides a test of whether those profiles can be understood in terms of classical physics—particle, momentum and energy balance plus the heat conduction relation—with the exception that the transport coefficients and the radial electric field and rotation velocities taken from experiment may be produced in part by 'non-classical,' or anomalous, effects.

The principal results of these calculations for one of the five shot/timeslices considered are given in Figs. 1.a-d. Figure 1.a shows the experimental E_r^{exp}, $\upsilon_{\varphi c}^{exp}$, and $\upsilon_{\theta c}^{exp}$ profiles that were used as input, and the profiles of the calculated υ_{pinch} and $\upsilon_r = \Gamma_i/n_i$. It is clear from Fig. 1a that the negative (inward) peaking of υ_{pinch} just inside the separatrix produces (or at least is consistent with) a large negative pressure gradient just inside the separatrix. There is also a peaking of υ_r just inside the separatrix, produced by the ionization of the fueling and recycling neutrals, that enhances the magnitude of the negative pressure gradient just inside the separatrix, but this atomic physics effect is not as large as the effect of the peaking in υ_{pinch}. Similar results were obtained in the other four discharges considered.

The two principal conclusions indicated by these results are: 1) the pedestal structure observed in the edge of H-mode (and some L-mode) plasmas is a natural consequence of the constraints imposed by the conservation of particle, momentum and energy and the heat conduction relations, in the presence of an influx of recycling and fueling neutrals, for the experimentally observed radial electric field and

rotation velocities in the edge; and 2) the major cause of the edge pedestal structure is the large peaking in υ_{pinch} just inside the separatrix. The pinch velocity is caused primarily by the rotation velocity and the radial electric field; thus the remaining questions in understanding the pedestal structure would seem to be related to the causes of the observed rotation velocities and radial electric field in the edge plasma.

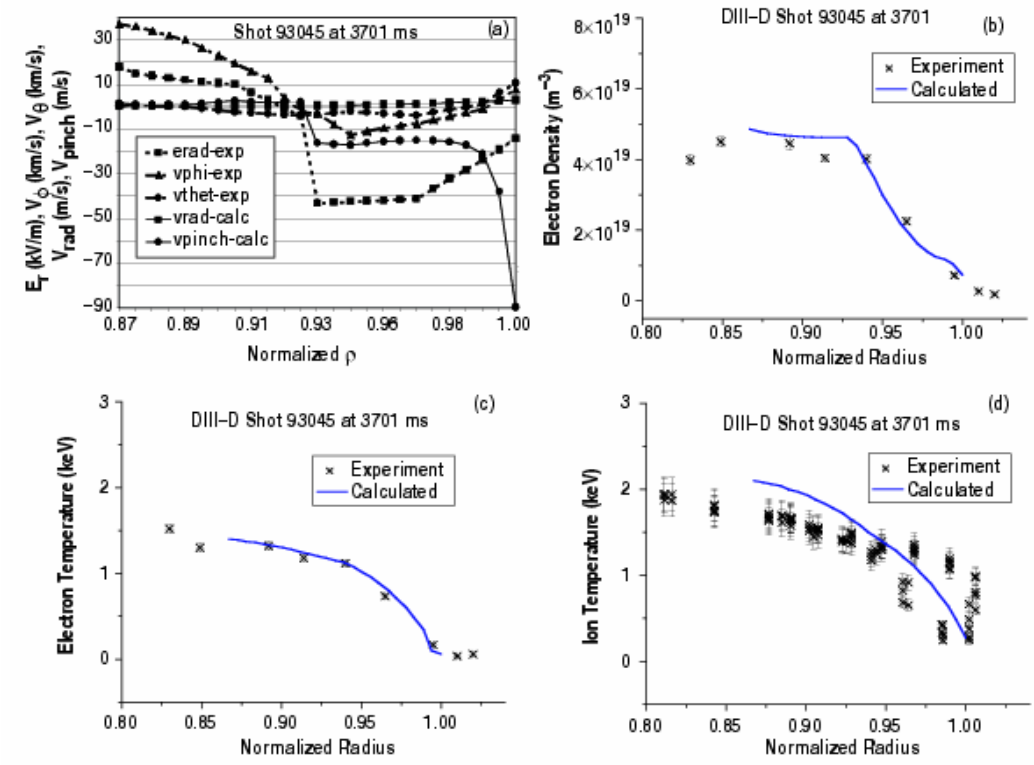

Figure 1: Edge pedestal profiles for DIII-D H-mode discharge 93045 calculated using experimental E_r, V_φ, V_θ and experimental separatrix boundary conditions : a) quantities involved in calculating the pressure gradient; b) calculated and measured n_e profiles; c) calculated and measured T_e profiles; d) calculated and measured T_i profiles.

The calculation for one discharge was repeated with the radial electric field and poloidal rotation velocities also being calculated from momentum balance. The calculated profiles were in somewhat better agreement with the measured profiles than when the experimental values of the radial electric field and poloidal rotation velocities were used in the calculation. Thus, it may well be that both the density and temperature profile pedestal structure and the associated radial electric field and rotation velocity profiles in the plasma edge are natural consequences of classical physics--particle, momentum and energy conservation and the heat conduction relations—but this remains to be established by a more extensive investigation.

3. References for Edge Pedestal

1. A.E. Hubbard, Plasma Phys. Controlled Fusion, 42, A283 (2000).
2. M. Kotschenreuther, W. Dorland, Q. P. Liu, *et al.*, Proc. 16th Conf. Plasma Phys. Control Fusion Research (Montreal, 1996) (IAEA, Vienna, 1997), Vol. 2, p.371.
3. J. E. Kinsey, R. E. Waltz and D. P. Schissel, Proc. 24th EPS, Berchtesgarten, 1997, Vol. III, p. 1081.
4. R. L. Miller, Y. R. Lin-Liu, T. H. Osborne and T. S. Taylor, Plasma Phys. Control. Fusion, 40, 753 (1998).
5. J. W. Connor, R. J. Hastie, H. R. Wilson and R. L. Miller, Phys. Plasmas, 5, 2687 (1998).
6. H. R. Wilson and R. L. Miller, Phys. Plasmas, 6, 873 (1999).
7. B. N. Rogers and J. F. Drake, Phys. Plasmas, 6, 2797 (1999).
8. P. B. Snyder, H. R. Wilson, J. R. Ferron, *et al.*, "Modification of High-Mode Pedestal Instabilities Based on Coupled Peeling-Ballooning Modes", Phys. Plasmas, 9, 2037 (2002).
9. P. B. Snyder, H. R. Wilson, J. R. Ferron, *et al.*, Nucl. Fusion, 44, 320 (2004).
10. R. J. Groebner and T. H. Osborne, Phys. Plasmas, 5,1800 (1998).
11. T. H. Osborne, J. R. Ferron, R. J. Groebner, *et al.*, Plasma Phys. Control. Fusion, 42, A175 (2000).
12. W. Suttrop, O. Gruber, B. Kurzan, *et al.*, Plasma Phys. Control. Fusion, 42, A97 (2000).
13. J. R. Ferron, M. S. Chu, G. L. Jackson, *et al*., Phys. Plasmas, 7, 1976 (2000).
14. T. Onjun, G. Bateman, A. H. Kritz, *et al.*, Phys. Plasmas, 9, 5018 (2002).
15. F. L. Hinton and G. M. Staebler, Phys. Fluids B, 5, 1281 (1993).
16. W. M. Stacey, Phys. Plasmas, 9, 3082 (2002).
17. K. C. Shaing and E. C. Crume, Phys. Rev. Lett., 63, 2369 (1989); K. C. Shaing, E. C. Crume and W. A. Houlberg, Phys. Fluids B, 2, 1492 (1990).
18. A. B. Hassam, T. M. Antonsen, J. F. Drake and C. S. Lui, Phys. Rev. Lett., 66, 309 (1991).
19. P. N. Gudzar, R. G. Kleva, R. J. Groebner and P. Gohil, Phys. Plasmas, 11, 1109 (2004).
20. W. M. Stacey, Phys. Plasmas, 8, 4073 (2001).
21. R. J. Groebner, M. A. Mahdavi, A. W. Leonard, et al., Phys. Plasmas, 9, 2134 (2002).
22. W. M. Stacey and R. J. Groebner, Phys. Plasmas, 10, 2412 (2003).
23. R. J. Groebner, M. A. Mahdavi, A. W. Leonard, et al., Nucl. Fusion, 44, 204 (2004).
24. W. M. Stacey, Phys. Plasmas, 11, 1511 (2004).
25. R. J. Groebner, M. A. Mahdavi, A. W. Leonard, *et al.*, Nucl. Fusion, 44, 204 (2004).
26. C. S. Chang, S. Ku and H. Weitzner, Phys. Plasmas, 11, 2649 (2004).
27. W. M. Stacey, "Structure of the edge density pedestal in tokamaks", Phys. Plasmas, to be published (2004).
28. W. M. Stacey, "Edge pedestal structure", Phys. Plasmas, submitted (2004).
29. G. D. Porter, R. Isler, J. Boedo and T. D. Rognlien, Phys. Plasmas, 7, 3663 (2000).
30. A. Kallenbach, Y. Andrew, M. Beurskens, *et al.*, Plasma Phys. Control. Fusion, 46, 431 (2004).
31. G. W. Pacher, H. D. Pacher, G. Janeschitz, *et al.*, Plasma Phys. Control. Fusion, 46, A257 (2004).
32. W. M. Stacey, "An edge pedestal model based on transport and atomic physics", Phys. Plasmas, 8, 4073 (2001).
33. W. M. Stacey, "An edge pedestal model", Contrib. Plasma Phys., 42, 283 (2002).
34. W. M. Stacey, "An edge pedestal investigation for high-confinement tokamak plasmas", Phys. Plasmas, 9, 1332 (2002).
35. W. M. Stacey and R. J. Groebner, "A framework for the development and testing of an edge pedestal model: formulation and initial comparison with DIII-D data", Phys. Plasmas, 10, 2412 (2003).
36. W. M. Stacey, "Investigation of transport in the DIII-D edge pedestal", Phys. Plasmas, 11, 1511 (2004).

37. W. M. Stacey, "Particle transport and density gradient scale lengths in the edge pedestal", Contrib. Plasma Phys., 44, 100 (2004).
38. W. M. Stacey, "Structure of the edge density pedestal in tokamaks", Phys. Plasmas, to be published (2004).
39. W. M. Stacey, "Edge pedestal structure", Phys. Plasmas, to be published (2004).
40. W. M. Stacey and R. J. Groebner, "Application of a particle, momentum and energy balance model to calculate the structure of the edge pedestal in DIII-D", Phys. Plasmas, to be submitted (in internal review) (2004).

C. THERMAL INSTABILITIES IN THE PLASMA EDGE

1. Background

A number of phenomena are routinely observed in tokamak plasmas in which an equilibrium or slowly evolving set of density and temperature distributions suddenly undergoes an abrupt transition to a quite different set of density and temperature distributions. Perhaps the most dramatic of these abrupt transitions is the collapse of the radial temperature profile, accompanied by the contraction of the current channel, leading to large-scale MHD activity and disruption. The collapse of the radial temperature distribution leading to these 'density limit' disruptions has been identified as a thermal instability in the radial energy and particle balances driven by low-Z radiation cooling in the plasma edge[1-3].

Another familiar example of a thermal instability is MARFE formation, in which a poloidally uniform temperature and density distribution in the plasma edge just inside the LCFS suddenly evolves into a highly non-uniform edge plasma distribution characterized by a poloidally localized and highly radiating region of high density and low temperature, usually located on the low-field inboard side in limited discharges and near the x-point in diverted discharges. This abrupt transition has been identified as a thermal instability in the density, momentum and energy balance along the field lines just inside the LCFS driven by either low-Z impurity radiation cooling[4] or charge-exchange and ionization cooling due to recycling neutrals[5].

Disruptions, MARFEs and other phenomena which can be understood as manifestations of thermal instabilities in the plasma edge or divertor appear to play a role in determining the maximum density that can be achieved in tokamaks. For example, in DIII-D diverted discharges, the following sequence is observed with continuous gas fueling[6-10]: 1) the plasma partially detaches from the outboard limiter and a dense, cool and highly radiating region forms just in front of the divertor plate; 2) at a somewhat later time, this dense, radiating region moves abruptly upstream in the divertor plasma to the vicinity of the x-point, forming a so-called 'divertor MARFE'; 3) with continued gas fueling, the confinement deteriorates and 4) a core MARFE is formed inside the separatrix in the vicinity of the x-point; 5) followed immediately by a H-L transition. On the other hand, ohmic heated and high-Z_{eff} auxiliary heated limited discharges in TEXTOR with continuous fueling tended to detach symmetrically when the radiated power reached 100% of the input power and then undergo a radiative collapse of the

temperature profile and disrupt[11], while auxiliary heated discharges and the low-Z_{eff} ohmic heated discharges tended to form MARFEs followed by a radiative collapse and disruption[12,13].

Thus, it seems clear that an understanding of thermal instability phenomena in the edge and divertor plasmas can make an important contribution to understanding a number of phenomena related to the density limit in tokamaks.

2. Work on Thermal Instabilities in Tokamak Edge Plasmas

For a number of years we have undertaken a systematic development of predictive onset conditions for various thermal instabilities in the plasma edge and the application of these predictions to understand various density-limiting phenomena in DIII-D. The predictive models for thermal instability onset have been incorporated into a code[14,15] for modeling the edge plasma conditions (core particle and power balances, 2-point divertor plasma model, 2D fueling and recycling neutral atom transport), This code uses whatever data that are available from experiment and calculates the other parameters (e.g. atomic physics reaction rates in edge and divertor plasmas) that are needed to evaluate the thermal instability onset predictions.

The development of a predictive onset condition for a particular thermal instability was developed by performing a linear stability analysis of the governing particle, energy and (in some cases) momentum balance equations for a specific type of perturbation about a given equilibrium solution to the governing equations. This led to a dispersion relation, from which a solution for the linear growth rate could be found, either analytically or numerically. The condition for the vanishing of the linear growth rate defined the threshold condition for the onset of the respective thermal instability. This threshold condition was then, when possible, solved for a threshold value of some parameter (e.g. the density) above which the thermal instability grew.

Collapse of radial temperature profile leading to disruption

The onset conditions for collapse of the radial temperature distribution leading to disruption were determined first from a simplified treatment of the radial distribution[16] and then with a distributed model[17] by evaluating the linear stability of the radial particle and energy balance equations in the edge and core to perturbations $\delta n \sim \delta T \sim J_0(5.5r/a)$ which represent a temperature decrease in the outer region $2.4 < r/a < 5.5$ and an increase in the inner region. The threshold condition can be expressed as a threshold line-averaged density above which a density limit disruption would be predicted. The threshold density increases with the thermal conductivity in the core and decreases with impurity radiation term, $f_z(-\partial L_z/\partial T)$. This radiative collapse onset calculation is routinely made in analyzing DIII-D shots, and the threshold density prediction is well above the measured density in those shots that do not disrupt. In the

half-dozen shots examined that did disrupt, the measured line-average density exceeded the threshold density late in the discharge.

MARFE Onset

The onset condition for MARFE formation was derived by considering the linear stability of the 3D particle, momentum and energy balance equations in a thin band just inside the LCFS to toroidally symmetric perturbations primarily along the field lines, but with small radial extent as well[18-24]. The onset condition could be expressed as a threshold edge plasma density, the value of which increased with the heat flux flowing radially across the edge, decreased with the concentrations of low-Z impurity and neutral atoms in the edge, and had a rather complicated temperature dependence reflecting the temperature dependence of the impurity radiation emissivity and the atomic physics cooling rates as well as an explicit 1/T dependence.

This MARFE onset condition, n_{marfe}, was evaluated for a number of times during several "density limit" discharges with continuous gas fueling in DIII-D[25-29]. It was found that the time at which the increasing value of the measured edge density became as large as the calculated MARFE threshold density was very close to the time at which the x-point MARFE formation was observed experimentally, as shown in Table 1. Similar discharges in which MARFEs were neither observed nor predicted are indicated by "none". (The divertor MARFE onset shown in this table will be discussed later.)

It is noted that the MARFE onset prediction has no explicit q_{95}-dependence. Yet it is clear from Table 1 that the line average density at which a MARFE occurred, normalized to the Greenwald density $n_{GW} = I/\pi a^2$, depended inversely on q_{95} and that this dependence was predicted. The likely explanation is that some of the measured edge parameters that were used to evaluate the onset prediction depend on the parallel path length of the scrape-off layer and divertor channel along the field lines and this path length can be characterized by $L_{\|} \sim q_{95;}$ e.g. the longer $L_{\|}$ the more radiative and recycling neutral cooling and the lower the edge temperature, other things being the same.

Divertor MARFE Onset

A prediction for the onset of divertor MARFEs was developed[30] by examining the stability of the one-dimensional particle, momentum and energy balance equations along field lines in the divertor plasma to perturbations along the field lines with scale length comparable to the distance from the divertor plate to the x-point. The resulting dispersion relation is sufficiently complicated that numerical evaluation is required to determine the growth rate. Examination of the dispersion relation indicates that impurity radiation, atomic physics cooling and the particle flux from the core into the SOL are destabilizing, while the heat flux from the core into the SOL and volumetric recombination are stabilizing.

Table 1: **MARFE onset prediction for gas-fueled DIII-D shots**
(R = 1.70-1.76 m, a = 0.6 m, κ = 1.70-1.75)

Shot #	P_{NB} (MW)	q_{95}	n/n_{GW} @ t_{marfe}	MARFE t_{marfe}^{exp} (s)	MARFE t_{marfe}^{calc} (s)	DIVMARFE $t_{divmarfe}^{exp}$ (s)	DIVMARFE $\omega_{div}>0$ (s)
92980	9.5	6.0	0.73	3.53	3.5-3.6		
92796	5.0	6.0	0.67	3.05-3.10	3.0-3.2	2.70-2.90	2.70-2.75
92983	2.5	6.0	0.58	2.90-3.00	2.6-2.8		
92972	5.0	3.0	0.95	3.05-3.15	3.0-3.2		
97979	6.5	3.8	0.81	None	None		
100308	4.5	3.1	0.96	None	None		
98893	2.0	3.5	1.40	None	None		
101560	4.6	4.2	0.79	4.80-4.90	4.8-4.9	4.65-4.80	4.50-4.80
101565	4.7	4.0	0.80	4.80-4.90	4.8	4.60-4.85	4.60-4.80
101626	3.4	4.2	0.81	None	None	None	None
101627	4.8	4.2	0.75	None	None	None	None
102447	4.5	4.0	0.79	4.90-4.98	4.8-4.9	4.70-4.90	4.80-4.90
102858	4.5	4.3	0.77	3.90-4.53	4.2-4.4	4.10	4.00-4.20
102859	4.7	4.1	0.74	4.10-4.25	4.0-4.2	4.10-4.30	4.0
102461	2.5	2.9	0.95	None	None		
102456	2.5	3.9	0.79	3.30-3.33	3.30-3.33		

The conditions in the divertor were evaluated for several DIII-D shots and the time intervals within which the linear growth rate became positive were determined for several DIII-D discharges and found to be in agreement with the times for which divertor MARFEs were observed experimentally, as indicated in Table 1.

Transport Enhancement

The possibility that transport enhancement associated with short radial wavelength thermal instabilities in the edge could be responsible for the L-H transition or for the H-mode confinement degradation observed experimentally was investigated[31-33] by performing a linear stability analysis of the particle, momentum and energy balance equations in the plasma edge to 2D (r, $\perp$) perturbations about an equilibrium solution.

A dispersion relation for the growth rates of thermal instability modes associated with ion and electron temperature instabilities of the form

$$\omega = -\frac{2}{3}\left(\chi\left(\nu L_T^{-2} + k_r^2\right) + \frac{5}{2}\nu\frac{\Gamma_\perp}{n}L_T^{-1} - \alpha \right), \qquad (1)$$

was found, where the radiation and atomic physics terms differed for the ions

$$\alpha_i = \frac{5}{2}(\nu - 1)\nu_{ion} + \frac{3}{2}\nu_{at}^c\left(\nu - \left[1 + \frac{T_i}{\nu_{at}^c}\frac{\partial \nu_{at}^c}{\partial T_i}\right]\right) - \frac{1}{n}\left(\nu\frac{H_i}{T_i} - \frac{\partial H_i}{\partial T_i}\right) \qquad (2)$$

and the electrons

$$\alpha_e = n_z\left(\frac{\nu L_z}{T_e} - \frac{\partial L_z}{\partial T_e}\right) + \nu_{ion}\left\{\frac{5}{2}(\nu - 1) + \nu\frac{E_{ion}}{T_e} - \left(\frac{3}{2} + \frac{E_{ion}}{T_e}\right)\frac{T_e}{\nu_{ion}}\frac{\partial \nu_{ion}}{\partial T} - \frac{1}{n}\left(\nu\frac{H_e}{T_e} - \frac{\partial H_e}{\partial T_e}\right)\right\}. \quad (3)$$

Here $\chi_r \sim T^{\nu}$ was used, $L_T^{-1} = -(dT/dr)/T$, and H is any external heating in the pedestal.

Assuming that the transport enhancement associated with these thermal instabilities can be represented by Kadomtsev's connection length expression $\Delta\chi \approx \omega k_r^{-2}$ and that the background transport in the absence of thermal instabilities is χ^0, Eq. (1) was solved for the threshold value of L_T for which $\omega = 0$. Using the heat conduction relation, this threshold L_T can be converted to a threshold for the non-radiative power crossing the separatrix

$$P_{thresh} = \frac{5}{4}\Gamma_r T A_{sep}\left[\sqrt{1 + \frac{\left(\chi^0\left(\alpha - \chi^0 k_r^2\right)/\nu\right)}{\frac{5}{4}\frac{\Gamma_r}{n}}} + 1\right] \quad (4)$$

where A_{sep} is the area of the separatrix.

The sum of $P_{threshi}$ for the ions and $P_{threshe}$ for the electrons was compared with the measured power crossing the separatrix, P_{sep}^{exp}, as shown in Table 2, for both L-H and H-L transitions with a wide range of edge conditions[34,35]. A value $k_r^{-1} = 1$ cm was used in the comparison because $\Delta\chi \approx \omega k_r^{-2}$ can exceed the representative H-mode thermal conductivity $\chi^0 \approx 0.1$ m^2/s for typical growth rates of $\omega > 10^3$/s. Clearly, there is agreement between the predicted power threshold of Eq. (4) and the measured power crossing the separatrix at the L-H and H-L transitions in these discharges, suggesting that the stabilization of $k_r^{-1} \approx 1$ cm thermal instabilities in the edge pedestal could be involved in triggering the L-H transition, and conversely that destabilization of $k_r^{-1} \approx 1$ cm thermal instabilities could be involved in triggering the H-L transition.

Table 2 **Some DIII-D shots just prior to the L-H or H-L transition** (R=1.71-1.79m, a=0.6m, κ=1.73-1.89, LSN divertor, $\chi^0 = 0.1$ m^2/s, $k_r^{-1} = 1$ cm)

Shot #	*Time (ms)*	*I (MA)*	*B (T)*	P_{NB} *(MW)*	n_{eped} *(e19/m^3)*	T_{eped} *(eV)*	P_{sep}^{exp} *(MW)*	P_{thr} *(MW)*
L-H								
102456	1725	1.4	2.0	2.6	3.22	95	1.55-1.86	1.54
97979	1900	1.4	2.0	2.0	2.59	125	1.72-2.04	2.18
92079	2275	1.0	2.1	6.8	1.28	220	3.99-4.06	4.00
84027	2575	1.3	2.1	1.1	2.94	144	1.28-1.36	1.13
H-mode								
97979[a]	3250	1.4	2.0	6.5	6.35	525	4.64-4.96	2.59
H-L								
92976	3210	1.0	2.1	5.0	4.95	275	3.96-4.33	4.21
101565	4950	1.4	2.0	4.7	6.75	170	4.21-4.85	4.60
102456	3500	1.4	2.0	2.4	6.25	150	2.48-2.82	2.36
102461	3300	1.4	1.5	2.4	7.80	170	2.11-2.17	2.18

[a] well into H-mode phase, not at the L-H of H-L transition—control case

It is widely observed in DIII-D H-mode discharges in which it is attempted to build up the density by continuous gas fueling that the energy confinement time and the steepness of edge pedestal density and temperature gradients all decrease with continued fueling. The destabilization and growth of short radial wavelength instabilities of the type discussed above, but with shorter radial wavelengths $k_r^{-1} < \sqrt{\chi^0/\omega}$ that would cause a much less dramatic transport enhancement, could be responsible for the observed deterioration of χ and L_T^{-1} in the edge pedestal. The above equations were evaluated[26] for the ion temperature instability growth rate at several times in some continuously gas fueled DIII-D discharges in which the energy confinement times were observed to deteriorate with time. The calculations were made for $k_r^2 << \nu L_T^{-2}$ so that k_r^2 could be neglected in Eq. (1). The increase with time of the calculated growth rate and the decrease with time of the measured $H_{89P} = \tau_{exp}/\tau_{iter89p}$ (based on the ITER-89P scaling law) appeared to be correlated.

A review[36] of thermal instabilities in tokamaks was prepared.

3. References for Thermal Instabilities

1. A. Gibson, Nucl. Fusion, 16, 546 (1976).
2. N.Ohyabu, Nucl. Fusion, 19, 1491 (1979
3. C. E. T. F. Ashby and M. H. Hughes, Nucl. Fusion, 21, 911 (1981).
4. J. F. Drake, Phys. Fluids, 30, 2429 (1987).
5. M. Z. Tokar, Phys. Scr. 31, 411 (1985).
6. T. W. Petrie, A. G. Kellman and M. A. Mahdavi, Nucl. Fusion, 33, 929 (1993).
7. T. W. Petrie, D. N. Hill, S. L. Allen, et al., Nucl. Fusion, 37, 321 (1997).
8. T. W. Petrie, S. L. Allen, T. N. Carlstrom, et al., J. Nucl. Mater., 241-243, 639 (1997).
9. R. Maingi, M. A. Mahdavi, T. C. Jernigan, et al., Phys. Plasmas, 4, 1752 (1997).
10. W. M. Stacey and T. W. Petrie, Phys. Plasmas, 7, 4931 (2000).
11. G. Waidmann and G. Kuang, Nucl. Fusion, 32, 645 (1992).

12. J. Rapp, P. C. De Vries, F. C. Schuller, et al., Nucl. Fusion, 39, 765 (1999).
13. U. Samm, P. Bogen, G. Esser, et al., J. Nucl. Mater., 220-222, 25 (1995).
14. W. M. Stacey, "A coupled plasma-neutrals model for divertor simulations", Phys. Plasmas, 5, 1015 (1998).
15. W. M. Stacey, "A calculation model for density limits in auxiliary heated, gas fueled tokamaks and applications to DIII-D model problems", Phys. Plasmas, 8, 3673 (2001).
16. W. M. Stacey, "Radial thermal stability of the radiative mantle", Phys. Plasmas, 3, 1012 (1996).
17. W. M. Stacey, "Density limits in tokamaks", Phys. Plasmas, 4, 1069 (1997).
18. W. M. Stacey, "Explanation for MARFE formation and subsequent evolution into a detached symmetric plasma edge", Phys. Plasmas, 3, 2673 (1996).
19. W. M. Stacey, "Multifaceted asymmetric radiation from the edge; impurity density limits in tokamaks with poloidal asymmetry and rotation", Phys. Plasmas, 3, 3032 (1996).
20. W. M. Stacey, "Multifaceted asymmetric radiation from the edge suppression by external edge heating", Phys. Plasmas, 4, 134 (1997).
21. W. M. Stacey, "Validity of the impurity entrainment assumption the thermal stability analysis of multifaceted asymmetric radiation for the edge in tokamak plasmas", Phys. Plasmas, 4, 242 (1997).
22. W. M. Stacey, "Thermal stability of the tokamak plasma edge", Plasma Phys. Control. Fusion, 39, 1245 (1997).
23. W. M. Stacey, "Density limits for multifaceted asymmetric radiation from the edge", Fusion Technol., 36, 38 (1999).
24. W. M. Stacey, "Effect of convection on multifaceted asymmetric radiation from edge density limits", Phys. Plasmas, 7, 3464 (2000).
25. W. M. Stacey, M. A. Mahdavi, R. Maingi and T. W. Petrie, "Multi-faceted asymmetric radiation from the edge formation in DIII-D high-confinement mode discharges with continuous gas puffing", Phys. Plasmas, 6, 3941 (1999).
26. W. M. Stacey and T. W. Petrie, "The role of thermal instabilities in limiting the density in DIII-D", Phys. Plasmas, 7, 4931 (2000).
27. W. M. Stacey, "A calculation model for density limits in auxiliary heated, gas fueled tokamaks and application to DIII-D model problems", Phys. Plasmas, 8, 3673 (2001).
28. W. M Stacey, T. W. Petrie and A. W. Leonard, "Thermal instability explanation of similar density limits in gas fueled DIII-D H-mode shots with different operating conditions", Phys. Plasmas, 9, 888 (2002).
29. W. M. Stacey, T. W. Petrie and T. H. Osborne, "Thermal instability analysis of different types of density limits in DIII-D gas-fueled, high-mode discharges", Phys. Plasmas, 9, 4174 (2002).
30. W. M. Stacey, "Detachment and divertor temperature and density redistribution", Phys. Plasmas, 8, 525 (2001).
31. W. M. Stacey, "Thermal Instabilities in the edge transport barrier", Phys. Plasmas, 6, 2452 (1999).
32. W. M. Stacey, "Edge pedestal deterioration in tokamak high-mode discharges", Phys. Plasmas, 8, 5199 (2001).
33. W. M. Stacey, "Spontaneous edge transport barrier formation due to suppression of edge thermal instabilities as a low-high trigger mechanisms in tokamaks", Phys. Plasmas, 9, 3082 (2002).
34. W. M. Stacey and T. W. Petrie, "Testing of an edge thermal instability model for the high-to-low mode power threshold", Phys. Plasmas, 10, 3949 (2003).
35. W. M. Stacey, "Testing of an edge thermal instability stabilization model for the low-to-high mode power threshold", Phys. Plasmas, 11, 686 (2004).
36. W. M. Stacey, "A review of thermal instabilities in tokamak plasmas", Nucl. Fusion, submitted (2004).

D. PLASMA ROTATION

1. Background

Plasma rotation in tokamaks is of interest because of its ability to stabilize the resistive wall mode by effectively making the wall more conductive[1], because of its potential to quench turbulent transport via flow shear[2], because of the effects of inertial forces on equilibria[3] and transport[4], and because of the insight that it can provide about transport mechanisms. There is a great deal of plasma rotation data for DIII-D, correlation analysis[5] of which suggests that the same physics governs momentum and ion energy

transport. Momentum transport is widely considered to be anomalous, because the familiar perpendicular neoclassical momentum transport[6-8] is too small by two orders of magnitude to agree with experimental momentum damping rates, but the less familiar gyroviscous momentum transport rate[9-17] is of the same order as inferred from experiment and has been found to agree with measured momentum confinement times in a number of tokamaks[18] as well as in DIII-D[19,20]. Calculation of momentum transport rates from gyro-fluid microinstability models are also under development[21].

2. Work on Plasma Rotation in DIII-D

Earlier work on the first-principle calculation of plasma toroidal and poloidal rotation, including a first-principle calculation of neoclassical gyroviscous momentum transport, was collected and extended to provide a basis for analysis of DIII-D rotation data[22,23]. Predicted momentum confinement times and rotation velocities are compared with experimental values in Table 3. With the exception of the last shot, which is the only one with an internal transport barrier, the gyroviscous prediction of the momentum confinement time is in agreement with the measured value, over a wide range of confinement modes and beam powers.

Table 3: Comparison of Predicted and Measured Toroidal Rotation Speeds and Momentum Confinement Times in DIII-D

Shot Time	Mode, NBI, impurity	P_{nbi} MW	$\overline{n}$ m^{-3}	T_{i0}, T_{e0} keV	$V_{\phi 0}$ / V_{thD}	τ_φ^{th} ms	τ_φ^{exp} ms	$V_{\varphi 0}^{th}$ 10^5m/s	$V_{\varphi 0}^{exp}$ 10^5m/s
98777 1.6 s	L, Co Carbon	4.5	3.42	3.5 2.5	0.31	80	73	1.52	1.50
98775 1.6 s	L, Co Neon	"	4.05	6.3 3.3	0.37	147	152	2.90	3.06
99411 1.8 s	H, Co Carbon	9.2	4.80	8.3 3.9	0.32	93	84	2.90	2.64
106919 2.0 s	QH, Ctr Ni-Cu,	9.32	2.58	10.9 3.9	0.40	44	45	3.86	3.98
" 3.5 s	"	"	2.83	14.2 4.2	0.38	64	68	4.21	4.48
106956 3.1 s	QDB Ctr CuNi,	11.77	3.75	15.1 4.4	0.24	44	46	2.41	2.51
102942 0.85 s	H, Co Carbon	4.89	2.36	1.8 2.5	0.40	55	51	2.20	2.02
" 1.25 s	ITB, Co Carbon	7.08	2.67	4.8 4.2	0.35	52	72	2.94	4.01

The radial distributions of the calculated toroidal and poloidal rotation velocities are compared with the measured rotation velocities of the carbon impurity species for one of the shots in Figs. 2 and 3. The gyroviscosity expression is the product of a constant depending on temperature, major radius and toroidal field, a factor Θ which depends on the calculated poloidal density asymmetries and the poloidal rotation velocities, and a factor G which depends on the radial density, temperature and velocity gradient scale lengths estimated from experimental data. The toroidal rotation calculation is shown for the best estimate of the factor ΘG and for a value twice as large. The agreement between the predicted and measured velocities is improved by enhancing the gyroviscous momentum transport rate, in this shot, perhaps indicating that some other transport mechanism is also involved.

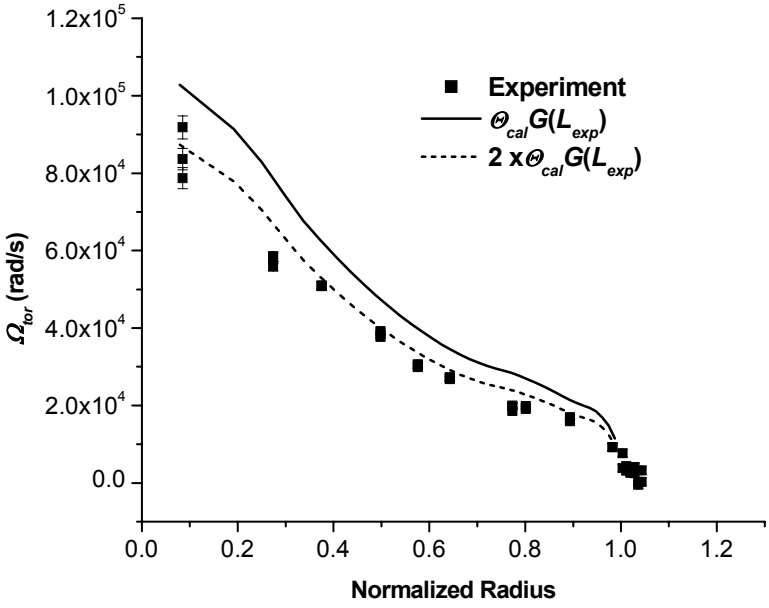

Figure 2: Comparison of the calculated toroidal angular velocity Ω_ϕ with experiment for different values of the product ΘG (DIII-D shot 98777 @ 1.6 s)

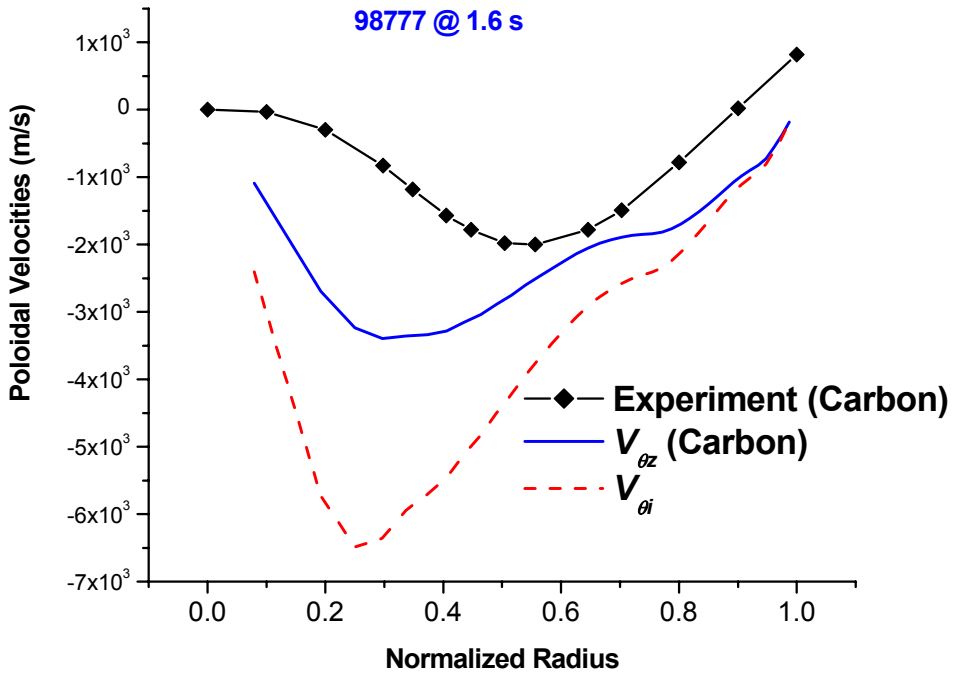

Figure 3: Comparison of the calculated poloidal velocities with experiment. (DIII-D shot 98777 @ 1.6 s)

We note that there has been some confusion on the existence and magnitude of neoclassical gyroviscosity. While the gyroviscous neoclassical theory is well documented[9-17], it is not so familiar as the perpendicular neoclassical momentum transport theory nor was it reported in three contemporary developments[6-8] of momentum transport theory based on gyroradius ordering schemes. In these gyroradius ordering developments[6-8], both the poloidal rotation and the gyroviscosity vanished to leading order. Further investigation of the gyroradius ordering development showed that a poloidal rotation velocity of the order seen experimentally and a non-vanishing gyroviscosity were obtained in the next order. Numerical calculations[18-20] demonstrated that, even though the velocity gradients in the gyroviscosity were smaller than those in the perpendicular viscosity, when the much larger coefficient of gyroviscosity was taken into account the gyroviscosity was two orders of magnitude larger than the perpendicular viscosity reported in these papers and should not be ordered out on the basis of the velocity gradients alone.

3. References on Rotation

1. A. M. Garofalo, et al., Nucl. Fusion, 41, 1171 (2001).
2. K. H. Burrell, Phys. Plasmas, 4, 1499 (1997).
3. E. Hameiri, Phys. Plasmas, 5, 3270 (1998).

4. W. M. Stacey, Phys. Plasmas, 8, 158 (2001).
5. J. S. deGrassie, et al., Nucl. Fusion, 43, 142 (2003).
6. F. L. Hinton and S. K. Wong, Phys. Fluids, 28, 3082 (1985).
7. J. W. Connor, et al., Plasma Phys. Control. Fusion, 29, 919 (1987).
8. S. K. Wong and V. S. Chan, Phys. Plasmas, 11, 3432 (2004).
9. A. N. Kaufmann, Phys. Fluids, 3, 610 (1960).
10. S. I. Braginskii, Rev. Plasma Phys., 1, 205 (1965).
11. A. B. Mikhailovskii and V. S. Tsypin, Sov. J. Plasma Phys., 10, 51 (1984).
12. W. M. Stacey and D. J. Sigmar, Phys. Fluids, 28, 2800 (1985).
13. R. H. Hazeltine and J. D. Meiss, "Plasma Confinement", Addison-Wesley, Reading MA (1994), pp 208, 220 and 226.
14. W. M. Stacey, Phys. Fluids B, 4, 3302 (1992).
15. A. L. Rogister, Phys. Plasmas, 1, 619 (1994).
16. H. A. Claassen, et al., Phys. Plasmas, 7, 3699 (2000).
17. A. N. Simakov and P. J. Catto, Phys. Plasmas, 10, 4744 (2003); also, Contrib. Plasma Phys., 44, 83 (2004).
18. W. M. Stacey and D. R. Jackson, Phys. Fluids B, 5, 1828 (1993).
19. W. M. Stacey and M. Murakami, Phys. Plasmas, 8, 4450 (2001).
20. W. M. Stacey and J. Mandrekas, Phys. Plasmas, 9, 1622 (2002).
21. G. M. Staebler, General Atomics, private communication (2004).
22. W. M. Stacey, "Neoclassical theory for rotation and impurity transport in tokamaks with neutral beam injection", Phys. Plasmas, 8, 158 (2001).
23. W. M. Stacey, "Neoclassical calculation of poloidal rotation and poloidal density asymmetries in tokamaks", Phys. Plasmas, 9, 3874 (2002).
24. W. M. Stacey and M. Murakami, "Momentum confinement in DIII-D shots with impurities", Phys. Plasmas, 8, 4450 (2001).
25. W. M. Stacey, "The role of neoclassical convection in the confinement improvement of plasmas with impurity injection in DIII-D", Phys. Plasmas, 8, 3689 (2001).
26. W. M. Stacey and J. Mandrekas, "Comparison of neoclassical rotation theory with experiment under a variety of conditions in DIII-D", Phys. Plasmas, 9, 1622 (2002).

D. NEUTRAL TRANSPORT

1. Background

The importance of neutral atoms to the performance of tokamak plasmas is widely recognized. Not only does the fueling of the core plasma by gas-injection and recycling depend on the transport of neutral particles through the plasma edge and divertor region, but a number of other important phenomena are sensitive to the neutral concentration in the plasma edge. For example, there is experimental evidence that the H-L transition, the density limit and the formation of the edge pedestal are all sensitive to the neutral concentration in the plasma edge.

Most codes presently available that can treat neutral transport in the complicated geometrical regions with strongly varying mean-free-path that characterize the edge and divertor regions of tokamaks are based on the Monte Carlo method. However, Monte Carlo calculations are very time consuming and their use, particularly in iterative, coupled plasma fluid—Monte Carlo neutrals calculations, is restricted. Moreover, the inherent numerical noise present in Monte Carlo simulations makes convergence difficult.

Thus, there is a need for a fast and accurate 2D neutrals code that can be used routinely for the analysis of tokamak experiments.

We have developed an interface current balance formulation of integral transport theory in which the transport of uncollided neutrals is treated exactly, while the effect of charge-exchange and elastic scattering across regions is treated approximately by means of escape probabilities[1]. The TEP methodology has been implemented into the 2D neutral transport code GTNEUT[2].

The TEP methodology and the GTNEUT code have been extensively tested by comparison with Monte Carlo[3] calculations for a series of model problems designed to be sensitive to the approximations made in the TEP methodology and its implementation in the current version of GTNEUT. These test comparisons[4-5] confirmed the basic TEP transport methodology over a wide range of the parameter Δ/λ, where Δ is the characteristic dimension of a computational region (equivalent to the grid size of a structured grid) and λ is the neutral mean-free-path.

2. Work on Neutral Transport in DIII-D

The TEP methodology has been an important component in several computational tools employed in the Georgia Tech – DIII-D collaboration. Simplified versions of the method have been implemented in the codes used in the first two research tasks described in this report. The full GTNEUT code has also been used to analyze DIII-D neutral density experiments[6] and to analyze and evaluate DIII-D pumping scenarios.

Analysis of DIII-D neutral density experiments

The neutral density in the vicinity of the X-point has recently been measured[7] in both L-mode and H-mode discharges in DIII-D. These discharges have been calculated with both GTNEUT and DEGAS, using the same 2-D geometry, the same background plasma properties (computed with the 2-D plasma fluid code B2.5), the same atomic reaction rate data, and the same carbon wall reflection model. Since the GTNEUT code cannot handle the transport of molecular species yet, the DEGAS code was run with and without molecular transport to facilitate the GTNEUT-DEGAS comparison.

First, we compared[6] the predictions of the GTNEUT and DEGAS codes with the experimental neutral measurements for the L-mode DIII-D discharge #96740 at 2250 ms. The geometric model is shown in Fig. 4. The X-point in this discharge was located 13.8 cm above the divertor floor. (The z-axis in Fig. (4) is arbitrary and does not correspond to the height over the divertor floor). The shaded cells in Fig. 4 correspond to the locations at which the neutral density measurements were made.

Typical plasma densities and electron temperatures in the regions just inside the separatrix (61-63 in Fig. 1) are in the range of 3.2×10^{19} – 1.4×10^{19} m^{-3} and 50-75 eV, respectively. Densities and

temperatures are considerably lower in the private flux regions. Molecules (transported in the DEGAS, but not the GTNEUT, simulations) emerge at a wall temperature of 0.025 eV (300 °K) while atomic neutrals (used in GTNEUT and in the DEGAS simulations without molecular transport) are assumed to have Franck-Condon energies of 1 eV. The same assumptions apply to the neutrals of the gas puffing source.

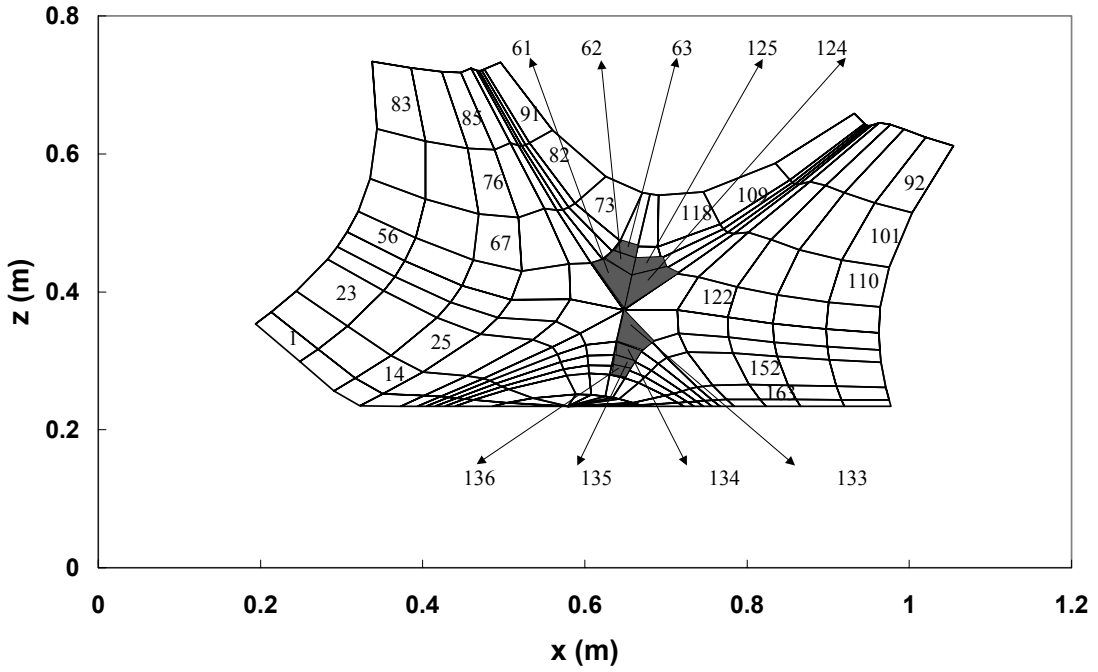

Figure 4 : Geometry used in the GTNEUT and DEGAS neutral transport simulations of DIII-D L-mode shot 96740 @ 2250 ms. Shaded regions correspond to locations where

The results of our GTNEUT and DEGAS simulations, as well as the experimental measurements and their error bars are shown in Fig. 5, where the various neutral densities are plotted vs. the height off the divertor floor. The region to the left of the separatrix line corresponds to the private flux area, and the region to the right is the core plasma.

It can be seen from Fig. 5, that the agreement between GTNEUT and the DEGAS case without molecular transport (solid circles) is excellent throughout the entire domain. The predictions of both codes (without molecular transport) agree with the experiment, being within the error bars of the measurements in all but one case. The DEGAS simulation including molecular transport under-predicts

the data in the private flux region, but is within somewhat better agreement with the measurements deep inside the plasma. These neutral measurements have also been calculated in agreement with experiment with a simplified TEP model[8] incorporated in the plasma analysis code described above.

Similar results have been obtained for the H-mode DIII-D discharge 96747 and are described in detail in Ref. 6.

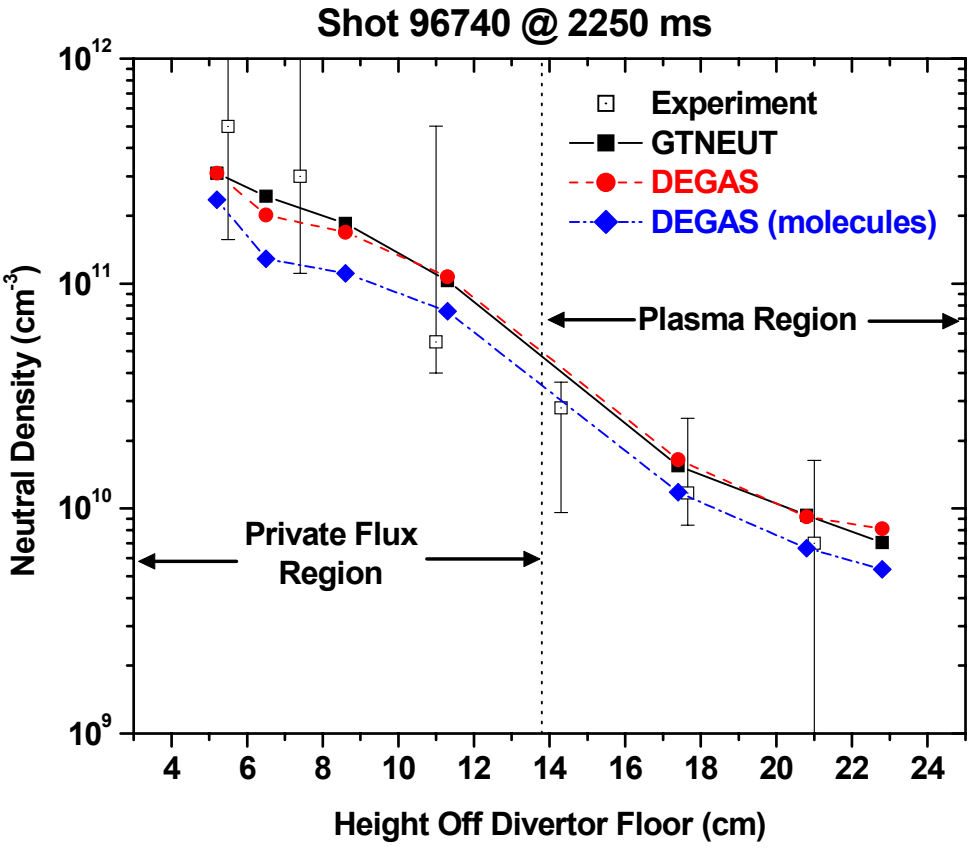

Figure 5: Comparison of GTNEUT and DEGAS simulations with experiment for the L-mode DIII-D shot 96749 @ 2250 ms.

Analysis of DIII-D pumping scenarios

GTNEUT was recently upgraded with new capabilities which greatly facilitated setting up and performing DIII-D related neutral transport simulations. These upgrades included: a) the implementation of a high performance sparse matrix solver for the solution of the resulting linear system of equations, which allows us to run much larger and therefore more realistic problems and b) the development of an

interface routine that can prepare the geometric part of the GTNEUT input file (which is the most laborious part) automatically by directly reading EFIT EQDSK files.

To test the capabilities of the upgraded code, we used it to calculate the exhaust rates from the dome and baffle pumps for the DIII-D shot 113026 @ 3000 ms (an upper single null discharge with dRsep ≈ 1.2, part of the AT Divertor Pumping series of experiments). The upper part of our geometry is shown in Fig.6 below. For the background plasma parameters (electron and ion densities and temperatures) inside the separatrix, we assumed poloidal symmetry and used the values obtained from GAProfiles. For the plasma parameters in the SOL above and below the X-point, we used experimental data provided by T. W. Petrie. For the regions where experimental data were unavailable (private flux region and the near-vacuum regions between the first wall and the last open flux surface) we used our judgment to assign arbitrary but reasonable background plasma parameters.

The results of our simulation predicted an exhaust rate ratio $\Gamma_{dome} / \Gamma_{baffle} = 0.88$. This result agrees very well with the measured ratio for dRsep = 1.2, as can be seen from Fig. 7.

The results of our neutral transport simulations depend on the ion and neutral recycling assumptions. Since no detailed information on the location and magnitude of the recycling sources was available for this shot, our reference simulation assumed in/out symmetry and equal recycling sources from the divertor segments adjacent to the dome and baffle pump entrances (wall segments 84, 86, 93, 95 in Fig. 6). This is a reasonable assumption given the flux expansion between the X-point and the strike points and the experimental indication of comparable recycling rates from inside and outside. The magnitude of the recycling sources was arbitrary (a crude estimate from the in/out ion flows at the pre-sheath) but this is not very important since we were interested in the ratio of the exhaust rates.

To test the sensitivity of our simulations to these uncertainties, the $\Gamma_{dome} / \Gamma_{baffle}$ ratio was calculated for different recycling assumptions ranging from uniform recycling (MCR or main chamber recycling) to various combinations of recycling flux ratios. These results are shown in Table 4. It can be seen that the $\Gamma_{dome} / \Gamma_{baffle}$ ratio is a sensitive function of the location of the recycling source.

It should be emphasized that our calculation was meant to demonstrate and test the new capabilities of our code and is not a definite calculation of the DIII-D pumping rates. We plan a more detailed series of simulations working in close contact with DIII-D scientists to ensure that we use the best information available on background plasma parameters and recycling sources.

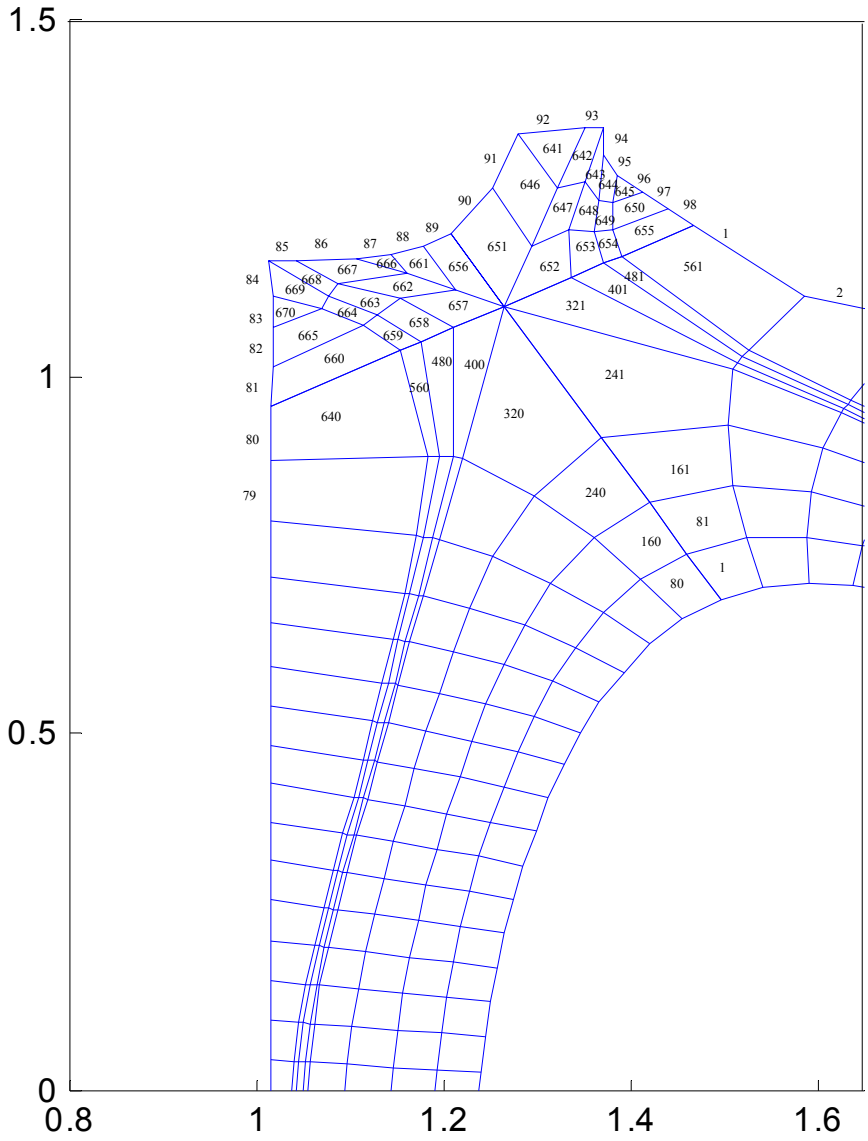

Figure 6: Upper part of DIII-D geometry used by GTNEUT for the analysis of DIII-D shot 113026 @ 3000 ms. The dome and baffle pump openings are represented by wall segments 85 and 94 respectively.

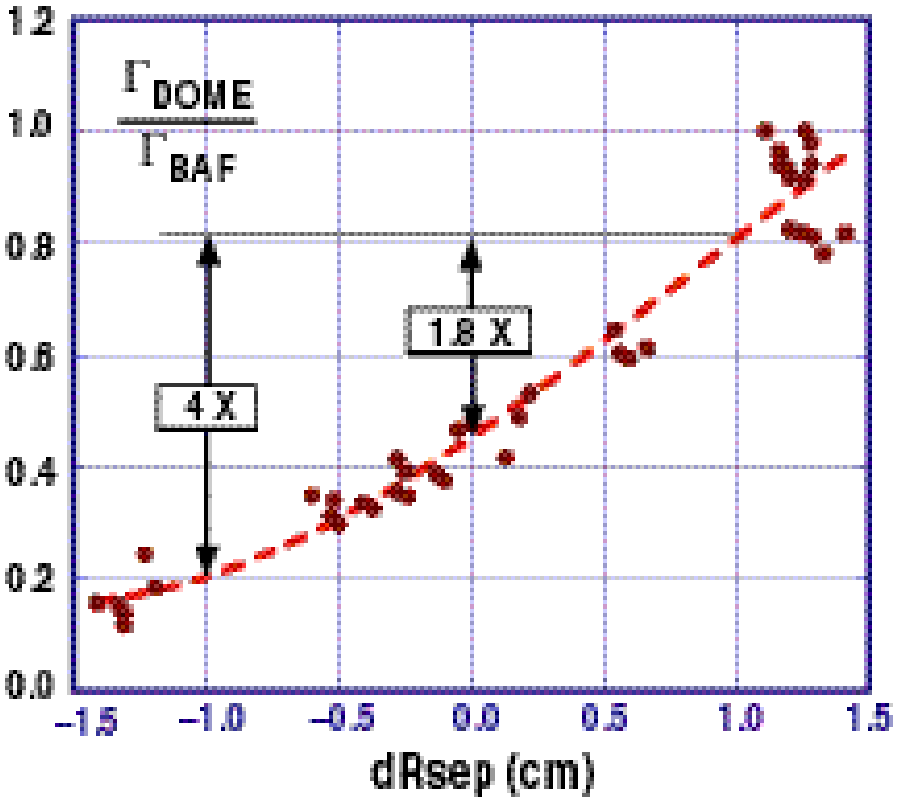

Figure 7*:* Experimental $\Gamma_{dome} / \Gamma_{baffle}$ ratio vs. dRsep (T.W. Petrie, et al.)

Flux distribution	Γ_{dome} (#/s)	Γ_{baffle} (#/s)	$\Gamma_{dome} / \Gamma_{baffle}$
$\Phi_{84} = \Phi_{86} = \Phi_{93} = \Phi_{95}$	0.5695×10^{22}	0.6426×10^{22}	0.88
Uniform (MCR)	0.613×10^{21}	0.71×10^{21}	0.86
$\Phi_{86} = \Phi_{93}$, $\Phi_{84} = \Phi_{95} = 0$	0.192×10^{22}	0.924×10^{22}	0.20
$\Phi_{86} = 1.5\times\Phi_{84}$ $\Phi_{93} = \Phi_{95}$	0.494×10^{22}	0.643×10^{22}	0.76
$(\Phi_{84}+\Phi_{86}) / (\Phi_{93}+\Phi_{95}) = 0.5$	0.380×10^{22}	0.855×10^{22}	0.45
$(\Phi_{84}+\Phi_{86}) / (\Phi_{93}+\Phi_{95}) = 2.0$	0.760×10^{22}	0.430×10^{22}	1.77

Table 4: Sensitivity of the ratio to various recycling assumptions. The total recycling source is kept constant for all cases and equal to 1.0×10^{23} #/s. Numerical subscripts correspond to the GTNEUT wall numbering scheme (see Fig. 6).

Two of the basic assumptions of the TEP methodology are the assumption of an isotropic neutral distribution function in both the inward and outward half-spaces at the interfaces between the computational regions, and the assumption of a uniform charge exchange collision source within the volume of each cell. The first assumption, also known as the DP_0 approximation, has been shown to be a good approximation since charge exchange and elastic scattering collisions tend to isotropize the neutral

distribution function. However, departures from anisotropy are possible, especially in long mean free path regions where anisotropies driven by wall reflection, presence of vacuum regions, pumps, etc. would persist across regions. Extending the original DP_0 approximation to include linearly (DP_1) and quadratically (DP_2) anisotropic distributions appears to resolve this issue, as evidenced by comparisons with Monte Carlo for model problems designed to accentuate the anisotropy effects[9].

The second assumption, i.e. the uniformity of the charge exchange collision source is embodied in the rational approximation that we employ for the first flight collision probability. This assumption may become questionable in regions where the neutral mean free path λ is much smaller than the characteristic dimension of the cell Δ. In these regions, the first collision source is predominantly located near the incident interface, resulting in a preferential backscattering of these neutrals across that incident surface. Work to address this problem is in progress as part of the Ph.D thesis of D-K. Zhang.

Finally, a long-term goal of our GTNEUT development is the coupling of our code with the 2D edge fluid code UEDGE[10]. Preliminary results show that the implementation of GTNEUT into UEDGE will improve UEDGE's treatment of neutral transport[11].

3. References for Neutral Transport

1. W. M. Stacey and J. Mandrekas, "A Transmission-Escape Probabilities Model for Neutral Particle Transport in the Outer Regions of a Diverted Plasma", Nucl. Fusion, 34, 1385 (1994).
2. J. Mandrekas, "GTNEUT: A code for the calculation of neutral particle transport in plasmas based on the Transmission and Escape Probability method," Comput. Phys. Comm. 161, 36 (2204).
3. Heifetz, D., Post., D., Petravic, D., et al., J. Comput. Phys. 46, 309 (1982).
4. W. M. Stacey, J. Mandrekas and R. Rubilar, "Interface Current Integral Transport Methods for the Calculation of Neutral Atom Transport in the Edge Region of Fusion Plasmas", Fusion Sci. Technol., 40, 66 (2001).
5. R. Rubilar, W. M. Stacey and J. Mandrekas, "Comparison of the TEP Method for Neutral Particle Transport in the Plasma Edge with the Monte Carlo Method", Nucl. Fusion, 41, 1003 (2001).
6. J. Mandrekas, R. J. Colchin, W. M. Stacey, et al., "Analysis of Recent DIII-D Neutral Density Experiments", Nucl. Fusion 43 (2003) 314.
7. Colchin, R.J., et al., Nucl. Fusion 40, 175 (2000).
8. W. M. Stacey, "Modeling the neutral density in the edge of the DIII-D plasma", Nucl. Fusion, 40,965 (2000).
9. Dingkang Zhang, J. Mandrekas and W.M. Stacey, "Extensions of the TEP Neutral Transport Methodology", Contrib. Plasma Phys. 44, 45 (2004).
10. F. Wising et al., Contrib. Plasma Phys. 36, 136 (1996).
11. J. Mandrekas, M.V. Umansky, D. Zhang, "Comparative study of neutral transport models for edge plasmas,' to be presented at the 46th APS DPP meeting, 2004.

E. IMPURITY TRANSPORT

1. Background

During our participation in the ITER EDA, we developed advanced computational tools for the analysis of impurity transport in tokamak plasmas. This involved the implementation of a multi species and multi charge state impurity transport module into our time-dependent 1½-D core transport code GTWHIST[1-3]. While the original motivation for this work was to perform coupled, self-consistent main plasma – impurity transport simulations in order to determine the feasibility of an impurity-seeded radiating mantle as a mechanism for the reduction of the exhaust power from the plasma core, the computational capability that was developed is useful in any situation involving external or intrinsic impurities in a plasma.

2. Previous Work on Impurity Transport under Grant ER54538

Analysis of RI-mode DIII-D Discharges

During the Georgia Tech – DIII-D Collaboration, we used these computational tools to analyze several DIII-D discharges with non-intrinsic seeded impurities (Ne, Ar and Kr)[4]. Although the original motivation for the injection of external impurities into DIII-D had been edge profile modification for AT operation, recent observations (in DIII-D and other tokamaks worldwide) of significant confinement improvement following impurity injection due to suppression of core turbulence have made impurity seeding an important tool for the understanding of transport mechanisms in tokamak plasmas and for the comparison of theory-based turbulence and transport models with experiment.

Most of our recent effort was in the analysis of a series of L-mode, negative shear, DN discharges exhibiting various degrees of confinement improvement in most transport channels following impurity injection (shots 98775-98794 and 103205-103209). This confinement improvement has been attributed to the synergistic effect of impurity induced enhancement of the $E \times B$ shearing rate and reduction of the drift wave turbulence growth rate[5].

Our coupled main plasma – impurity transport simulations were predictive in nature (in the sense that our transport code was run in predictive mode, not making any use of measured plasma or impurity profiles) but with a small number of adjustable coefficients (mainly amplitudes of the plasma and impurity charge state transport coefficients, strength and location of impurity source, etc.). We found that using simple empirical and semi-empirical transport models for the transport of the impurity charge states and the main plasma particle and energy transport, we were able to obtain very good agreement between simulation and experiment. A typical comparison between simulation and experiment is shown in Fig. 8, where various profiles from our simulation are compared with the experimental measurements for the Neon injected shot 98775.

Our simulations indicated that, while energy transport was reduced to almost neoclassical levels in these impurity seeded discharges, impurity transport was not neoclassical. In addition, we concluded

that the observed reduction of the Carbon concentration in the core was due to the reduction of the wall carbon source rather than due to transport effects.

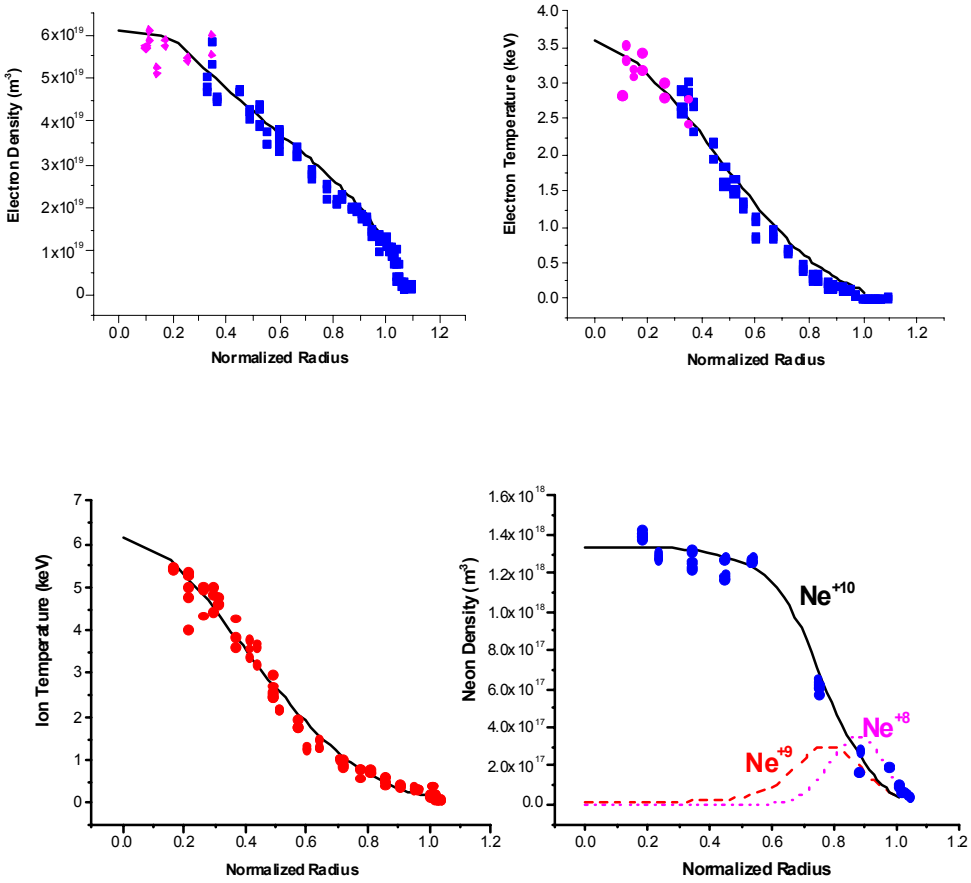

Figure 8: Comparison of simulation and experiment for various main plasma and impurity profiles for shot 98775 at 1.6 s.

The results of our simulations were useful not only because they helped us understand impurity transport in DIII-D, but also because they provided us with self-consistent Z_{eff} profiles (including the contribution from all charge states and not only from the ones that were measured) as well as with profiles of the various impurity charge states. This profile information was then used as input to gyrokinetic or gyrofluid codes to make quantitative tests of theory-based turbulence models with experimental measurements[5-6].

Neoclassical Impurity Transport Analysis of QDB Discharges

A series of multi-species impurity transport simulations using the neoclassical impurity transport code NCLASS[7] were performed in order to determine whether the observed strong high-Z impurity accumulation in recent Quiescent Double Barrier (QDB) DIII-D discharges (shots 106919 and 106972) is consistent with the predictions of neoclassical theory.

The simulations were performed for a fixed background plasma, using fits to the various measured profiles (n_e, T_e, T_i, various impurity charge states for C^{+6}, $Ni^{24\text{-}28}$, etc.). The various MHD metric coefficients required by NCLASS have been computed using the appropriate EFIT EQDSK files ("g" files) for this shot.

The total neoclassical particle flux and its various components for the Ni^{+26} state at t = 3510 ms for shot #106919 are shown in Fig. 9. Shown in Fig. 9 are the total flux, the banana-plateau (BP) flux, the Pfirsch-Schlüter (PS) flux, the classical (CL) flux and the flux due to the $\langle \mathbf{E} \cdot \mathbf{B} \rangle$ term. It can be seen that the dominant term is the BP term, as expected since Ni^{+26} is in the banana-plateau regime.

Comparison of the calculated particle fluxes and the associated transport coefficients with the experiment revealed that the measured pinch velocities and diffusivities were much higher than the neoclassical calculations except for the very center of the plasma at $\rho < 0.1$. This would suggest that high-Z impurity transport is not described by neoclassical processes in these QDB discharges.

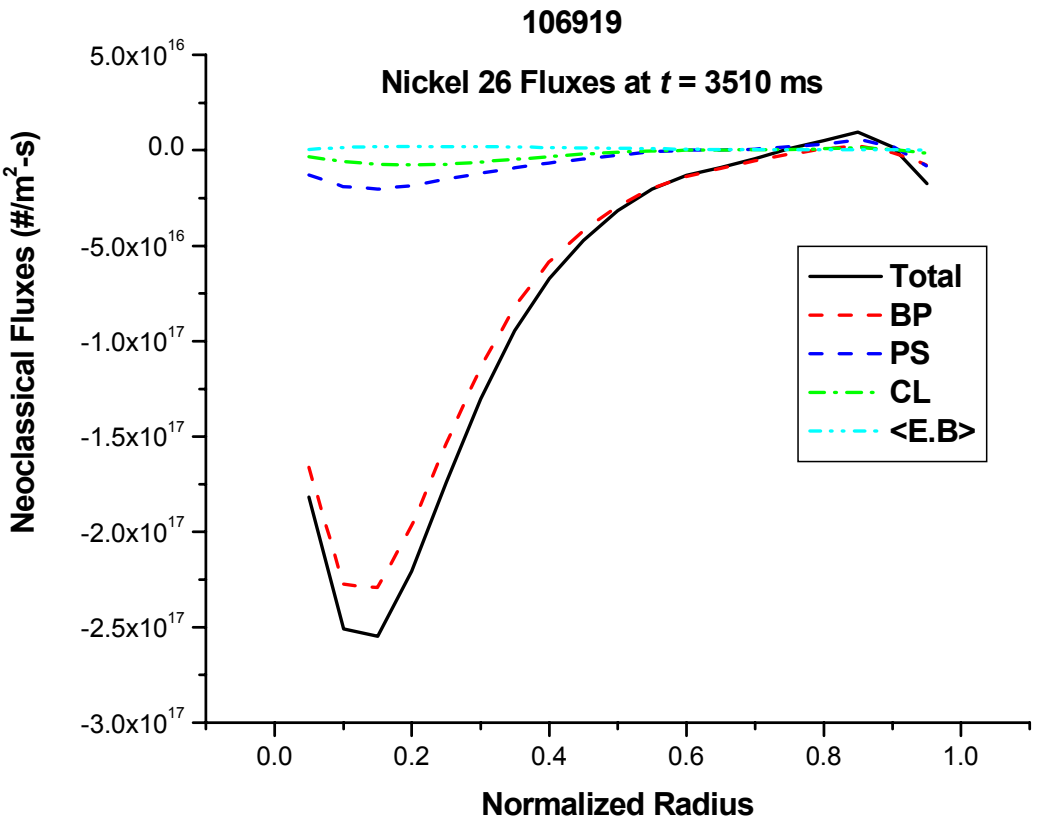

Figure 9: Total neoclassical flux and components for the Ni^{+26} charge state at 3510 ms.

3. References for Impurity Transport

1. J. Mandrekas, W.M. Stacey, *Nucl. Fusion* **35** (1995) 843.
2. J. Mandrekas, W.M. Stacey, F.A. Kelly, *Nucl. Fusion* **36** (1996) 917.
3. J. Mandrekas, W.M. Stacey, F.A. Kelly, *Nucl. Fusion* **37** (1997) 1015.
4. J. Mandrekas, W.M. Stacey, M. Murakami, M.R. Wade, G.L. Jackson, *Contrib. Plasma Phys*., **40** (2000) 498.
5. M. Murakami, et al., *Nucl. Fusion* **41** (2001) 317.
6. M. Murakami, et al. *Physics of Confinement Improvement of Plasmas with Impurity Injection in DIII-D*, 18th IAEA Fusion Energy Conference, Sorrento, Italy, 2000.
7. W.A. Houlberg, K.C. Shaing, S.P. Hirshman, and M.C. Zarnstorff, Phys. Plasmas **4** (1977) 3230.
8. W. P. West, M.R. Wade, C.M. Greenfield, et al. *Phys. Plasmas*, **9** (2002) 1970.

II. NEXT-STEP OPTION PHYSICS (Grant ER54350)

A. SUMMARY

For more than a decade we have been involved in physics and design analysis of possible next-step tokamak options, including first ITER, later FIRE and most recently a tokamak neutron source for a near-term transmutation reactor for burning the transuranics in spent nuclear fuel. We have also recently supported the National Transport Code Coordination activity under this grant. In recent years, much of the effort has been devoted to defining the physics and performance characteristics required of a tokamak fusion neutron source that could drive a sub-critical reactor for the transmutation of the transuranics in spent nuclear fuel. This document provides a final report for the activity in each of these areas for the last grant period.

B. SUB-CRITICAL TRANSMUTATION REACTORS WITH A TOKAMAK FUSION NEUTRON SOURCE

1. Background

At the present rate of nuclear power production in the USA the accumulation of spent nuclear fuel (SNF) discharged from the reactors in the "once-through" fuel cycle will require the opening of a new high-level waste (HLW) repository on the Yucca Mountain scale about every 30 years. The repository requirements can be greatly (an order of magnitude or more) reduced (and the nuclear fuel utilization can be increased) if the plutonium and higher transuranics in the SNF is recycled and used as fissionable fuel in other reactors designed for that purpose, since the decay heat of these transuranics is the principal constraint on the volume of spent fuel that can be stored in a repository. Studies over the past decade or so[1-3] confirmed the technological feasibility of spent fuel transmutation and have identified the potential advantage of sub-critical reactors driven by neutron sources for this purpose. Accelerator-spallation neutron sources have been extensively studied for this application, but relatively little effort has been devoted to investigating the application of fusion neutron sources.

2. Previous Work on Transmutation Reactor Fusion Neutron Sources under Grant 54350.

For the past several years we have investigated the required characteristics of a tokamak D-T neutron source to drive a sub-critical reactor for the purpose of the transmutation of spent nuclear fuel, vis-à-vis the existing tokamak plasma physics and fusion technology database, with the objective of developing a tokamak neutron source that will be prototyped by ITER. The investigation has included the conceptual design of fast-spectrum, sub-critical transmutation reactors that are compatible with the tokamak neutron source geometry and that are based on the nuclear, fuel, materials and separation

technologies that are being investigated in the DoE Nuclear Energy Programs; i.e the Generation-IV and Advanced Fuel Cycle Initiatives and the Advanced Nuclear Fuel Development Program. In order to insure a close integration of our work on the definition of the tokamak neutron source requirements with this nuclear technology being developed being in the Nuclear Energy Program, we have 1) interacted with other Georgia Tech faculty who are working on advanced fuels and actinide separations systems; 2) interacted with scientists at the Argonne and Oak Ridge National Laboratories and at the Idaho National Engineering Laboratory who are working on the GEN-IV, AFCI and Advanced Fuels programs; and 3) involved these people in a series of student-faculty conceptual design projects of transmutation reactors to insure the compatibility of the tokamak neutron source concepts being developed under this grant with nuclear technology being developed under the GEN-IV, AFCI and Advanced Fuels Programs. This work is documented below and summarized in the attached paper.

Documentation of work on transmutation tokamak neutron sources under Grant 54350

a. W. M. Stacey, "Capabilities of a D-T Tokamak Fusion Neutron Source for Driving a Spent Nuclear Fuel Transmutation Reactor", Nucl. Fusion, 41, 135 (2001).
b. W. M. Stacey, J. Mandrekas, E. A. Hoffman, et al., "A Fusion Transmutation of Waste Reactor", Fusion Sci. Technol., 41, 116 (2002).
c. W. M. Stacey, J. Mandrekas, E. A. Hoffman, et al., "A Fusion Transmutation of Waste Reactor" *Fus. Eng. & Des.*, 63-64, 81 (2002).
d. E. A. Hoffman and W. M. Stacey, "Nuclear and Fuel Cycle Analysis for a Fusion Transmutation of Waste Reactor", *Fus. Eng. & Des.*, 63-64, 87 (2002).
e. A. N. Mauer, W. M. Stacey, J. Mandrekas and E. A. Hoffman, "A Superconducting Tokamak Fusion Transmutation of Waste Reactor", Fusion Sci. Technol., 45, 55 (2004).
f. E. A. Hoffman and W. M. Stacey, "Nuclear Design and Analysis of the Fusion Transmutation of Waste Reactor", Fusion Sci. Technol., 45, 51 (2004).
g. J. Mandrekas, L. A. Cottrill, G. C. Hahn and W. M. Stacey, "FTWR-AT: An Advanced Tokamak Neutron Source for a Fusion Transmutation of Waste Reactor", Georgia Tech report GTFR-167 (2003).
h. E. A. Hoffman and W. M. Stacey, "Comparative Fuel Cycle Analysis of Critical and Sub-critical Fast Reactor Transmutation Systems", Nucl. Technol., 144, 83 (2003).
i. W. M. Stacey, "Transmutation Missions for Fusion Neutron Sources", Fusion Engr. Des., to be published (2004).
j. W. M. Stacey, V. L. Beavers, W. A. Casino, et al., "A Sub-Critical , Gas-Cooled Fast Transmutation Reactor (GCFTR) with a Fusion Neutron Source", Nucl. Technol., to be published (2004).
k. W. M. Stacey, J. Mandrekas and E. A. Hoffman, "Sub-critical Transmutation Reactors with Tokamak Fusion Neutron Sources", Fusion Sci. Technol., to be published (2005).

Attachment 1

SUB-CRITICAL TRANSMUTATION REACTORS WITH TOKAMAK FUSION NEUTRON SOURCES

W. M. Stacey[1], J. Mandrekas[1] and E. A. Hoffman[2]

[1]Fusion Research Center
Georgia Institute of Technology
Atlanta, GA 30332, USA

[2]Nuclear Engineering Division
Argonne National Laboratory
Argonne, IL 60439, USA

ABSTRACT

The principal results of a series of design scoping studies of sub-critical fast transmutation reactors (based on the nuclear and processing technology being developed in the USDoE Generation IV, Advanced Fuel Cycle and Next Generation Nuclear Plant programs) coupled with a tokamak fusion neutron source (based on the ITER design basis physics and technology) are presented.

I. INTRODUCTION

For many years there has been a substantial R&D activity devoted to closing the nuclear fuel cycle. During the 1990s this activity emphasized the technical evaluation of reducing the requirements for long-term geological high-level waste repositories (HLWRs) for the storage of spent nuclear fuel (SNF) by transmutation (fission) of the plutonium and higher transuranics in the spent fuel discharged from fission power reactors[1-8]. Recycling of this SNF in thermal spectrum fission power reactors, the most obvious option, was found to not significantly reduce the HLWR requirements[1,2], because the destruction of transuranics (by neutron fission) would be offset by the production of more transuranics by neutron capture transmutation of the isotope ^{238}U that constitutes about 95% of (slightly enriched) thermal reactor fuel. Repeated recycling of the SNF in special purpose fast spectrum reactors was found to be more effective, but with the net destruction rate of transuranics still limited by the requirement for the presence of ^{238}U to provide a negative reactivity coefficient for safety and by a safety-related limit on the transuranics loading. There is a potential to relax these two safety-related limits if the reactor is operated sub-critical, with a neutron source making up the neutron deficit to sustain the neutron chain reaction. A general consensus emerged from these studies that significantly higher transuranics net destruction rates could be achieved in sub-critical reactors[1,2].

The accelerator community was quick to recognize the opportunity to use a D+ accelerator with a spallation target as a neutron source for a sub-critical transmutation reactor. Almost all of the studies in the 1990s of sub-critical transmutation reactors were based on an accelerator-spallation neutron source[1-8]. In the USA, these studies and the supporting R&D development were organized by DoE under the Accelerator Transmutation of Waste (AWTR) Program[6], which has now evolved into the Advanced Fuel Cycle Initiative[9] (AFCI).

The USDoE Generation IV (GEN-IV) nuclear reactor development activity[10] envisions that the pacing item for the development of a transmutation reactor--the development of the spent fuel processing technology--should be sufficiently advanced by about 2020 that the detailed design of a critical fast transmutation reactor and the associated processing facility could be started, which would enable the entire system to be brought online in about 2030. The roadmap[6] for developing sub-critical transmutation reactors driven by accelerator-spallation neutron sources also envisions such a reactor coming online in about 2030.

A sub-critical transmutation reactor (using the same nuclear and separations technology) driven by a tokamak fusion neutron source could be brought online somewhat later. The pacing items in bringing online a tokamak neutron source to drive a sub-critical transmutation reactor would be the operation of ITER (or a similar facility) as a prototype and the operation of a set of fusion technology test facilities needed to develop component reliability. ITER is scheduled to operate from 2015 to 2035. Component test facilities could be upgraded or constructed to operate before and in parallel with ITER, so it would be plausible to begin detailed design of a tokamak neutron source in about 2025. Construction of a sub-critical reactor using the same fast reactor technology developed for critical reactors and a tokamak fusion neutron source could then begin as early as about 2030, leading to initial operation in about 2040.

The fusion community has been rather slower in examining the opportunity of using a fusion neutron source for a sub-critical transmutation reactor, with only a few studies[11-16] through the end of the 1990s. Since that time we have undertaken at Georgia Tech a series of studies[17-24] of coupling a tokamak fusion neutron source based largely on ITER design basis physics and technology[25] with a

sub-critical transmutation reactor based on the nuclear and processing technology being developed in the USDoE GEN-IV, AFCI and NGNP programs[9,10,26].

II. THE FTWR AND GCFTR STUDIES

We have examined sub-critical transmutation reactors based on two of the nuclear technologies being developed in the GEN-IV studies. The Fusion Transmutation of Waste Reactor (FTWR) series of studies was based on a fast-spectrum reactor using a metal fuel consisting of TRU (transuranics) alloyed with zirconium in a zirconium matrix and cooled by a liquid metal (Li17Pb83 eutectic), which also served as the tritium breeder. The ongoing Gas Cooled Fast Transmutation Reactor (GCFTR) series of studies is based on a fast-spectrum reactor using TRU-oxide fuel in coated TRISO particle form in a SiC matrix cooled by He. Both the FTWR and GCFTR cores are annular and located outboard of the toroidal plasma chamber. The core plus plasma chamber were surrounded first by a reflector and then by a shield to protect the magnets from radiation damage and heating, as indicated in Fig. 1 for the initial FTWR design.

A design objective was to use near-term nuclear technology being developed in the DoE Nuclear Program (GEN-IV, AFCI, NGNP) and near-term fusion technology being developed in the ITER Project. The ANL metal fuel, liquid metal cooled reactor designs[8] were adapted to accommodate a different coolant and TRU-Zr fuel for the FTWR designs. The fast, gas-cooled reactor designs being developed under the GEN-IV Program guided the choice of the GCFTR core design, and the coated fuel particle technology being developed in the NGNP program[26] was adapted to accommodate TRU-oxide fuel for the GCFTR.

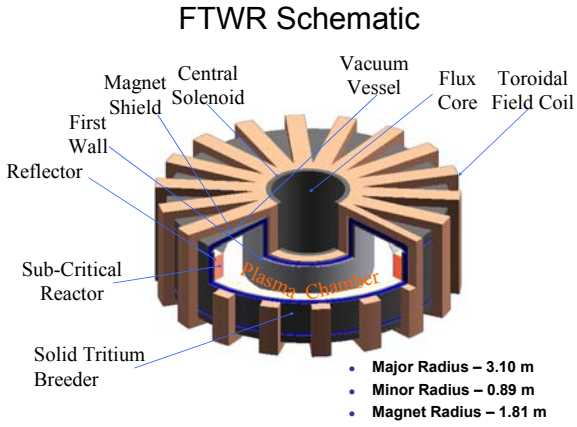

Fig. 1 Tokamak Fusion Transmutation of Waste Reactor

The fusion technology was based on the ITER design[25]. The superconducting magnet design was based directly on the ITER superconducting magnet system. The first-wall and divertor designs were based on adaptations of the ITER designs to accommodate different coolants. The reference materials compositions for the FTWR and GCFTR designs are given in Table I.

TABLE I Reference Materials Composition of FTWR and GCFTR

Component	FTWR	GCFTR
Reactor		
Fuel	TRU-Zr metal in Zr matrix	TRU TRISO/SiC matrix (option BISO/Zirc-4 matrix)
Clad/structure	FeS/FeS	Zirc-4/FeS
Coolant	LiPb	He
Trit. Breeder	LiPb	LiO_2
Reflector	FeS, LiPb	FeS, He
Shield	FeS, LiPb, B_4C, ZrD_2, W	W, B_4C, He
Magnets	NbSn,NbTi/He (OFHC/LN_2)	NbSn, NbTi/He
First-Wall	Be-coated FeS, LiPb	Be-coated FeS, He
Divertor	W-tiles on Cu-CuCrZr, LiPb	W-tiles on Cu – CuCrZr, He

A series of design studies was performed for the FTWR. The objectives of the original FTWR study[18] were to achieve minimum size by using liquid nitrogen cooled Cu magnets, to achieve electrical power breakeven (Q_e = 1), and to achieve an adequate transmutation rate to dispose of the spent nuclear fuel being generated by three 1000 MW_e LWRs. The second FTWR-SC study[19] was a modification of the FTWR design to replace the Cu magnets with superconducting magnets and to

provide enough shielding to make them lifetime components. The core radius became larger as a result, and the power density was held constant so that the FTWR nuclear and thermal core design[18,24] and fuel cycle analysis[18,23] could be simply scaled up by volume. The third FTWR-AT study[20] investigated the reduction in size that could be achieved in a superconducting design by using advanced tokamak physics; again the same core power density was used.

The GCFTR series of studies is now in progress. The objectives of the first GCFTR study[22] were to achieve > 90% burnup of transuranics in the coated fuel particles without reprocessing the coated TRU pellets, achieve an adequate transmutation rate to dispose of the spent nuclear fuel being generated by three 1000 MW_e LWRs, and to achieve net electric power while avoiding the very high temperatures (and associated materials requirements) characteristic of other gas-cooled reactor designs. During the later stages of the GCFTR study it became apparent that the superconducting magnet thicknesses could be reduced, and the preliminary GCFTR-2 study was performed to assess the effect on the design.

The major dimensions of the various design concepts are given in Table II. The plasma-related parameters for the FTWR and GCFTR designs are given in Table III.

TABLE II Dimensions (m) of FTWR and GCFTR Designs

Parameter	FTWR[a]	FTWR-SC[b]	FTWR-AT[c]	GCFTR[d]	GCFTR-2[d]
Major Radius[e], R_0	3.10	4.50	3.86	4.15	3.70
Fluxcore, R_{fc}	1.24	1.10	0.65	0.66	0.66
CS+TF, Δ_{mag}	0.57	1.68	1.20	1.50	1.13
Refl+Shld, Δ_{rs}	0.40	0.65	0.90	0.86	0.82
Plasma, a_{plasma}	0.89	0.90	1.10	1.04	1.08
Core					
Inner Radius, R_{in}	4.00	5.40	5.00	5.25	4.84
Width, W	0.40	0.40	0.40	1.12	1.12
Height, H	2.28	2.28	2.28	3.00	3.00

[a]ITER physics, LN_2 Cu magnets, PbLi/TRU-metal reactor[18]; [b] ITER physics, ITER SC magnets, PbLi/TRU-metal reactor[19]; [c] AT physics, SC magnets, PbLi/TRU-metal reactor[20]; [d] ITER physics, ITER SC magnets, He/TRU-TRISO reactor[22]; [e] Includes gap, first-wall, scrape-off layer and items below.

The requirements on β_N and confinement are within the range routinely achieved in present experiments, and the requirements on β_N, confinement, energy amplification Q_p, and fusion power level are at or below the ITER level. The requirement on the current-drive efficiency, after calculation of bootstrap current fraction using ITER scaling, is only somewhat beyond what has been achieved to date (γ_{CD} = 0.45 in JET and 0.35 in JT60-U). The ongoing worldwide tokamak program is addressing the current-drive/bootstrap current/steady-state physics issue. The current-drive efficiency/bootstrap fraction needed for FTWR/GCFTR is certainly within the range envisioned for Advanced Tokamak operation and may be achieved in ITER.

III. TRANSMUTATION REACTOR CORES

III.A. FTWR

The fuel is a transuranic zirconium alloy (TRU-10Zr) dispersed in a zirconium matrix and clad with a ferritic steel similar to HT-9. The relative amounts of transuranics and zirconium in the fuel region are adjusted to achieve the desired neutron multiplication (k_{eff} = 0.95) at the beginning of each cycle. At equilibrium, the transuranics will constitute approximately 45% of the fuel volume. The annular transmutation reactor core is outboard of the plasma, and both are surrounded by reflector and shield (Fig. 1). The design of the FTWR transmutation reactor is based on the ANL ATW blanket design studies[8]. The same pin and assembly geometry was used, with the exception that the length of the assembly was increased to 228 cm. Table IV gives the basic data for the fuel assembly design. The reactor core is 40 cm thick and consists of 470 assemblies, 1/5 of which will be 'half assemblies' placed in the gaps along the interior and exterior surfaces of the reactor region to produce a more uniform annular distribution, as shown in Fig. 2.

The total coolant mass flow rate required to maintain T_{in} = 548 K and T_{out} = 848 K is 51630 kg/s. The required pumping power is 130 MW, the majority of which is needed to overcome MHD losses.

TABLE III Tokamak Neutron Source Parameters for Transmutation Reactors

Parameter	FTWR[a]	FTWR-SC[b]	FTWR-AT[c]	GCFTR[d]	GCFTR-2[d]	ITER[e]
Fusion power, P_{fus} (MW)	≤ 150	≤ 225	≤ 500	≤ 180	≤ 180	410
Neutron source, $S_{fus}(10^{19}$ #/s)	≤ 5.3	≤ 8.0	≤ 17.6	≤ 7.1	≤ 7.1	14.4
Major radius, R (m)	3.1	4.5	3.9	4.2	3.7	6.2
Aspect ratio, A	3.5	5.0	3.5	4.0	3.4	3.1
Elongation, κ	1.7	1.8	1.7	1.7	1.7	1.8
Current, I (MA)	7.0	6.0	8.0	7.2	8.3	15.0
Magnetic field, B (T)	6.1	7.5	5.7	6.3	5.7	5.3
Safety factor, q_{95}	3.0	3.1	3.0	3.0	3.0	
Confinement, $H_{IPB98}(y,2)$	1.1	1.0	1.5	1.0	1.0	1.0
Normalized beta, β_N	≤ 2.5	≤ 2.5	4.0	2.0	2.0	1.8
Plasma Power Mult., Q_p	≤ 2.0	≤ 2.0	4.0	2.9	3.1	10
CD efficiency,γ_{cd} $(10^{-20}$ A/Wm$^2)$	0.37[f]	0.23	0.04	0.5	0.61	
Bootstrap current fraction, f_{bs}	0.40[f]	0.50	≥0.90	0.35	0.31	
Neut. flux, Γ_n (MW/m^2)	≤ 0.8	≤ 0.8	≤ 1.7	≤ 0.9	≤ 0.6	0.5
Heat flux, q_{fw} MW/m^2)	≤ 0.34	≤ 0.29	≤ 0.5	≤ 0.23	≤ 0.23	0.15
Availability (%)	≥ 50	≥ 50	≥ 50	≥ 50	≥ 50	

[a–d] same as Table II; [e] ITER design parameters. (Ref. 25); [f] bootstrap current calc. using ITER scaling, then required CD effic. calculated.

TABLE IV FTWR Fuel Assembly Design

Pin Diameter (cm)		0.635
Clad thickness (cm)		0.05588
Pitch		Triangular
Pitch to Diameter		1.727
Pins per assembly		217
Structure Pins		7
Fuel Smear density		85%
Hexagonal Assembly Pitch		16.1
Assembly Length (cm)		228
Assemblies		470
Pumping Power (MW)		130
Volume %	Fuel	17.01
	Structure	10.44
	Coolant	69.55
Materials	Fuel	TRU-10Zr/Zr
	Structure	FeS
	Coolant	Li17Pb83

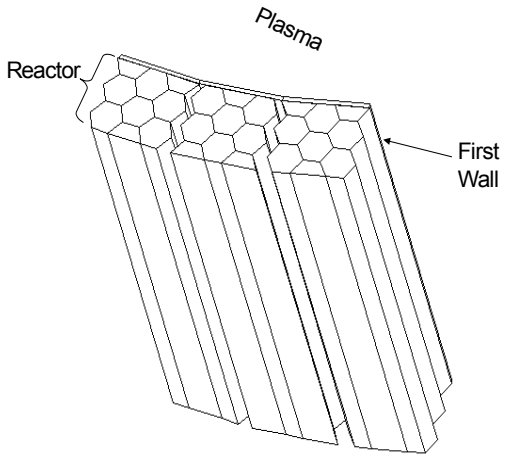

Fig. 2 FTWR Transmutation Reactor Core Configuration Outboard of Plasma Chamber

III.B. GCFTR

Design concepts were developed for a TRISO (tri-material isotropic) particle and for a BISO (bi-material isotropic) particle, as shown in Fig. 3.

The TRISO particle has a TRU kernel (300 μm diameter) surrounded by a 50% porous buffer layer (100 μm) of ZrC to allow for fission product recoil and to accommodate fission product gas buildup, followed by a structural layer (20 μm) of pyrolytic carbon which prevents chlorine attack of the kernel during the coating process and contains the fission products, followed by a structural layer (25 μm) of SiC which shrinks under irradiation to provide an inward pressure to counteract the fission product gas pressure buildup, followed by an outer pyrolytic carbon layer (35 μm) to prevent interaction of the SiC

with any metallic cladding material. The BISO particle has a similar kernel and buffer layer followed by a (25 μm) pyrolytic carbon structural layer and then by a (35 μm) ZrC structural outer layer.

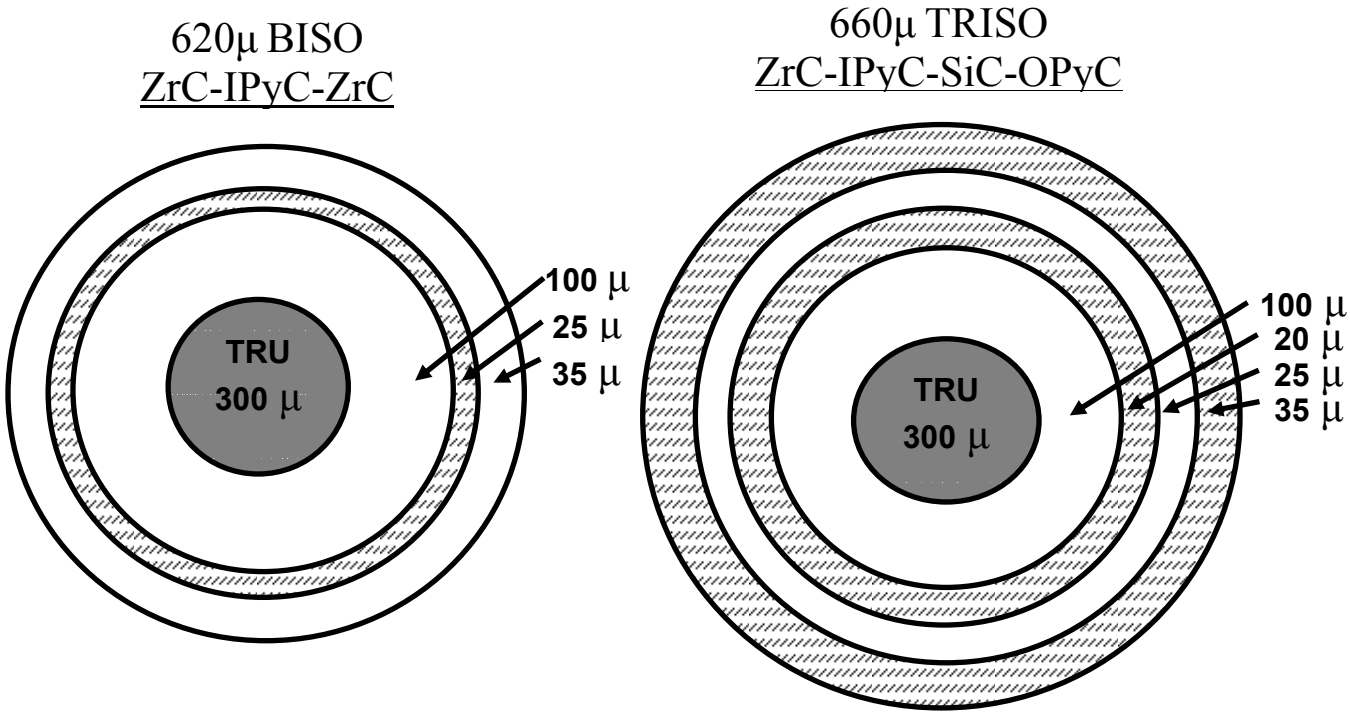

Figure 3: BISO and TRISO coated fuel particles

It is an objective to achieve very high burnup before loss of integrity of the coated fuel particle or degradation of fission product gas containment becomes unacceptable. The TRISO and BISO particles are predicted to reach 155 MPa at 90% FIMA and 180MPa at 99% FIMA for the maximum predicted fuel centerline temperature of 560 ^{o}C. The operational pressure limit due to the compressive yield strength of SiC for the TRISO particle is 345 MPa, and the similar limit for the BISO particle is 352 MPa. These limits correspond to fuel centerline temperature limits of 1700 and 1520 ^{o}C at 90% FIMA and 99% FIMA, respectively, for the BISO particle; and to fuel centerline temperature limits of 1690 and 1510 ^{o}C at 90% FIMA and 99% FIMA, respectively, for the TRISO particle.

A thermal analysis was performed for Zirc-4 clad pins in which the BISO fuel particles were uniformly homogenized in the Zirc-4 matrix material. A configuration with 207200 fuel pins 0.60 cm in radius with a gap of 0.005 cm and a 0.057 cm thick cladding was chosen for the analysis. For 3000 MW_{th} total reactor power uniformly distributed in the fuel pins, the volumetric heat source is q''' = 42.2 MW/m^3. With a He mass flow rate of 2870 kg/s, the He coolant entered at 280 C and exited at 481 C, the maximum clad temperature was 513 C (well below the 1845 ^{o}C m. p. for Zircaloy), the maximum homogenized fuel centerline temperature was 560 C, well below the 2000+ ^{o}C melting point for TRU-oxides, and the He pumping power was 0.15 MW. A He coolant v/o ≥ 25% would be adequate for heat removal under normal operating conditions.

IV. FUEL SEPARATION AND FABRICATION SYSTEMS

IV.A. FTWR

The processing system for the FTWR will be identical to the waste processing system being developed for the ATW system[27]. The waste processing system consists of three basic components. The first is a uranium extraction system (UREX) that will separate the bulk uranium and fission products in the SNF from the transuranic elements. The transuranic elements and the rare earth fission products will then be transferred to a pyro-metallurgical system (Pyro-A) that will separate the rare earths from the transuranic elements and convert the latter to a metallic form for fuel manufacturing. The discharged FTWR fuel will be sent to a separate

pyro-metallurgical system (Pyro-B) where the residual actinides will be recovered. The recovered materials from Pyro-A and Pyro-B will be blended together and manufactured into new fuel elements for the FTWR.

The UREX system is assumed to remove 99.995% of the uranium and all of the fission products that are not rare earth elements. The Pyro A system is assumed to remove 95% of the rare earth fission products and recover 99.9% of the transuranic elements. The Pyro B system is assumed to remove 95% of the rare earth fission products, remove 100% of all other fission products, and recover 99.9% of the transuranic elements. In addition to the recovery fractions, the total fraction of transuranics that end up in the waste stream is a strong function of fractional burnup achieved during each residence in the FTWR. For the FTWR, each MTU of SNF will result in 70 g of transuranics in the waste stream.

IV.B. GCFTR

Aqueous systems for separating the TRU in LWR spent nuclear fuel (SNF) and systems for fabricating it into coated particle fuel have been identified for the GCFTR. The uranium (99.995%) is first removed from the SNF using a UREX process. The remaining 0.005% of the uranium, the TRU and the fission products are then treated with a TRUEX process and a TRU/lanthanide separation step to remove virtually all of the fission products, which are sent to a high-level waste repository. The TRU emerging from the TRUEX process (including 0.005% of the uranium and virtually all of the transuranics) is then fabricated into coated TRU fuel particles. The heavy metal composition of the 'TRU' emerging from this process is (U—0.43%, Np—4.32%, Pu—84.91%, Am—10.21%, Cm—0.13%).

The fabrication process starts with evaporation of the TRU stream, which is then passed through a calciner to form a mixture of transuranic oxides. Finally, a ZrC buffer layer and the pyrolytic carbon and ZrC (BISO) or pyrolytic carbon and SiC (TRISO) layers are coated onto the particles. Less than 0.1% TRU loss is assumed during the fabrication process.

V. FUEL CYCLE ANALYSIS

The composition changes in the fuel cycle were calculated with the REBUS fuel cycle code[28]

V.A. FTWR

The reference fuel cycle assumes that the FTWR fuel will remain in the reactor for 4 cycles of 623 days each and then be reprocessed, blended with 'fresh' SNF and fabricated into new fuel elements for re-insertion into a FTWR. A beginning-of-cycle (BOC) transuranic loading of 27 MTU will produce k_{eff} =0.95, the largest value during the cycle. Over the 40 FPY plant life of the first generation of FTWRs, the original charge of LWR feed will be reprocessed 5 times.

The initial charge of the reactor and the first reload batch will require approximately 3500 MTU of LWR SNF to manufacture these fuel elements. Following this, approximately 190 MTU of LWR SNF will be processed in each subsequent 623-day cycle. A first generation FTWR will process approximately 74 MT of transuranics from LWR SNF, of which approximately 56% will be fissioned, 0.2% will be lost to the waste streams, and 44% will be used in a second generation FTWR.

The second and subsequent generations of FTWRs will use the fuel from the previous generation FTWRs and therefore operate in the equilibrium mode over their entire life. Repeated recycling of the discharged transuranics from FTWRs in successive generations of FTWRs will ultimately result in the destruction of 99.4% of the transuranics discharged from LWRs.

V.B. GCFTR

An emphasis in the GCFTR investigation was achieving sufficiently high (>90% FIMA) TRU burnup that the coated fuel particles can be burned and then removed from the reactor and directly deposited in a waste repository without the necessity of reprocessing. To this end, we again examined a multi-batch fuel cycle in which the reactivity decrease (from k = 0.95 at BOC) associated with fuel burnup was partially offset by an increase in neutron source strength over the burn cycle.

For the reference 5-batch, 600 day burn cycle, 8.2 year fuel cycle, the BOC TRU loading was 36 MT for the TRISO fuel and 47 MT for the BISO fuel. For both fuels, the BOC k_{eff} = 0.95 and neutron source $P_{fusion} \approx 40$ MW, and the end of cycle $k_{eff} \approx 0.81$ (0.87 for BISO) and neutron source $P_{fusion} \approx 170$ MW (107 MW for BISO). About 23% of the BOC TRU loading is fissioned in an 8.2 year fuel cycle. The fuel would have to be resident in the core for about 10 such fuel cycles to achieve 90% TRU burnup.

V.C. Performance

The FTWR and GCFTR cores are designed to operate at a nominal fission power level of 3000 MW_{th}, which corresponds to the fission of 1.1 metric

tons of TRU per EFPH. A typical 1000 MW_e LWR produces 0.36 metric tons of TRU per EFPY. Hence, one FTWR or GCFTR would be able to 'support' (burn the TRU discharged from) three 1000 MW_e LWRs.

The FWTR and GCFTR also produce electrical power. The original FTWR with Cu magnets has a large ohmic heat removal power requirement and was designed for electrical breakeven, but superconducting FTWRs would produce net electrical power, as the GCFTR does. Using a Brayton cycle with 32% thermal-to-electrical energy conversion efficiency to convert the 3000 MW thermal power, the gross electric power production of a GCFTR would be 1024 MW_e. The electrical power requirements for the operation of the GCFTR are 305 MW_e, leading to an electric power amplification factor of Q_e = 3.4 and a net electric power production of 719 MW_e.

V.D. Deployment

Availability of the transmutation reactor will determine the annual transmutation rate, hence the number of transmutation reactors needed to service the USA LWR fleet. The projected SNF transmutation rate is 100A MTU per year for both the FTWR and the GCFTR, where A is the availability. (The other design variants with somewhat higher power would have somewhat higher transmutation rates.) At the present level of nuclear power production in the US, about 100 LWRs produce about 2000 MTU of SNF per year. Thus, 20/A transmutation reactors would be needed to handle the annual SNF production, assuming the present level of nuclear power continues indefinitely. Operating at 50% availability, 40 sub-critical reactors would accomplish this transmutation mission. At 75% availability, only 25 would be needed.

VI. COMPONENT LIFETIMES

The design lifetime of the GCFTR is 40 years at 75% availability, or 30 EFPY. The magnet systems, shields, reflectors, etc. are designed as lifetime components. However, the reactor fuel and structure, the first-wall of the plasma chamber and the divertor will have to be replaced one or more times over the 30 EFPY because of radiation damage.

It is envisioned that the coated fuel pellets will be imbedded in a matrix material and clad in Zircalloy-4 fuel elements and arranged in fuel assemblies constructed of ferritic steel. The fuel elements will be left in the reactor for five consecutive 600 EFPD cycles, which requires that the clad not fail in this "residence" time, during which it will accumulate a fast (E > 0.1 MeV) neutron fluence of 4.2×10^{22} n/cm^2. We have not been able to determine the radiation damage lifetime of Zircalloy-4, but it is widely used as cladding in nuclear reactors.

The structural material of the fuel assembly will accumulate a fast neutron fluence of 1.9×10^{23} n/cm^2 over the 30 EFPY design lifetime. The estimated[29] radiation damage lifetime of ferritic steel is 80-150 dpa, or $1.5\text{-}3.0 \times 10^{23}$ n/cm^2, implying that the core fuel assembly structure may need to be replaced once over the 30 EFPY lifetime of the GCFTR.

When the fuel is removed from the reactor after its residence time, the cladding will be replaced, and the matrix material (SiC or Zircalloy-4) will be replaced if necessary, but the coated fuel pellets will be blended with "fresh" fuel pellets and re-fabricated into fuel elements to be re-inserted into another GCFTR. The objective is to repeatedly recycle the fuel pellets until they reach > 90% FIMA, without reprocessing. The fast neutron fluence will be 4.1×10^{23} and 8.2×10^{23} n/cm^2 at 90% and 99% FIMA, respectively. A fluence lifetime in this range is then a requirement of the coated particle fuel development program.

The first-wall of the plasma chamber and the plasma-facing part of the divertor will accumulate fast neutron fluences of 7.5 and 5.8×10^{23} n/cm^2 , respectively, over the 30 EFPY lifetime of the GCFTR. The radiation damage limit of the ferritic steel first-wall structure is $1.5\text{-}3.0 \times 10^{23}$ n/cm^2 , which implies that it will be necessary to replace the first-wall 2-4 times over the 30 EFPY lifetime of the GCFTR. Erosion of the divertor by the incident plasma ion flux will necessitate several replacements over the 30 EFPY lifetime of the GCFTR.

The superconducting magnets are shielded to reduce the fast neutron fluence to the superconductor and the rad dose to the insulators below their respective limits—10^{19} n/cm^2 fast neutron fluence for Nb^3Sn and 10^9 rads for organic insulators (10^{10} rads for ceramic insulators).

VII. TRANSMUTATION MISSION IN THE FUSION PROGRAM

A transmutation reactor can be driven by a tokamak fusion neutron source based on physics (H, β_N, Q_p, etc.) similar to or less demanding than that used for the ITER design, except for the need to achieve a higher bootstrap current fraction and/or higher current drive efficiency. This tokamak neutron source can be constructed with the fusion technology being developed for ITER, but will need

to achieve greater availability, hence have greater component reliability, than ITER. Achieving higher availability, which will require various component test facilities, must be addressed in the fusion development program, but would have a higher near-term priority if the transmutation mission were undertaken.

The reactor technology for the sub-critical reactor driven by the fusion neutron source would be adapted from the reactor (nuclear, fuel, cooling, separations, materials) technologies being developed in the nuclear program (e.g. GEN–IV, AFCI, NGNP), but these technologies must be modified to provide for the tritium breeding requirement. A fusion nuclear technology program would have to be revived with this goal. There is a need to develop a long-lived structural material, primarily for the fuel assemblies of the sub-critical reactor, but also for the first wall of the fusion neutron source.

The technical requirements for a tokamak fusion neutron source that would fulfill the transmutation mission are significantly less demanding than for an economically competitive tokamak electrical power reactor and somewhat less demanding than for a DEMO, as indicated in Table V.

Table V Requirements for a Tokamak Neutron Source, Electric Power Reactor and DEMO

Parameter	Transmutation	Electric Power[a]	DEMO[b]
Confinement $H_{IPB98}(y,2)$	1.0	1.5-2.0	1.5-2.0
Beta β_N	< 2.5	> 5.0	> 4.0
Power Amplification Q_p	< 3	> 25	> 10
Bootstrap Current Fraction f_{bs}	0.2-0.5	0.9	0.7
Neutron wall load (MW/m^2)	≤ 1.0	> 4.0	> 2.0
Fusion Power (MW)	≤ 200	3000	1000
Pulse length/duty factor	long/steady-state	long/steady-state	long/steady-state
Availability (%)	> 50	90	< 50

[a] ARIES studies (Ref. 30); [b] DEMO studies (Ref. 31)

VIII. CONCLUSIONS

A sub-critical transmutation reactor, based on adaptation of nuclear and separations technology presently being developed in the DoE Nuclear Energy Program to accomodate tritium breeding, and driven by a tokamak D-T fusion neutron source, based on the physics and technology presently being developed in the DoE Fusion Energy Sciences Program, could be online in 2040. The tokamak neutron source, which would be about R = 4 m in major radius and produce < 200 MW of D-T fusion power, could be designed on the basis of the existing plasma physics and fusion technology databases, with only a few modest extensions. The pacing items for the neutron source would be operation of a prototype plasma (e.g. ITER) experiment and component test facilities to gain the experience necessary to achieve > 50% availability in operation of the fusion neutron source.

ACKNOWLEDGMENT This work was supported in part by DoE grant DE-FG0296ER54350. The contributions of Profs. D. Tedder, J. Lackey and C. de Oliveira and of the students in the Georgia Tech NRE design projects to the development of the material in this paper are gratefully acknowledged.

REFERENCES

1. "First Phase P&T Systems Study: Status and Assessment Report on Actinide and Fission Product Partitioning and Transmutation", OECD/NEA, Paris (1999).
2. "Proc. 1st-5th NEA International Exchange Meetings", OECD/NEA, Paris (1990,92,94,96,98).
3. "Nuclear Wastes--Technologies for Separations and Transmutations", National Research Council, National Academy Press, Washington (1996).
4. C. D. Bowman, et al., "Nuclear Energy Generation and Waste Transmutation Using Accelerator-Driven Intense Thermal Neutron Source", *Nucl. Instr. Methods, **A320***, 336 (1992).
5. W. C. Sailor, et al., "Comparison of Accelerator-Based with Reactor-Based Nuclear Waste Transmutation Schemes", *Progress in Nuclear Energy, **28***, 359 (1994).
6. "A Roadmap for Developing Accelerator Transmutation of Waste (ATW) Technology", US Dept. Energy report DOE/RW-0519 (1999).
7. D. E. Beller, et al., "The U.S. Accelerator Transmutation of Waste Program", Nucl.

Instr. & Meth. Phys. Res., A, **463**, 468 (2001).
8. R. N. Hill and H. S. Khalil, "Physics Studies for Sodium Cooled ATW Blanket", Argonne National Laboratory report ANL/RAE/CP-105355 (2001).
9. AFCI websites http://www.nuclear.gov/afci and http://apt.lanl.gov.
10. GEN-IV roadmap website http://gif.inel.gov/roadmap/.
11. T. A. Parish and J. W. Davidson, "Reduction in the Toxicity of Fission Product Wastes through Transmutation with Deuterium-Tritium Fusion Neutrons", *Nuclear Technology, **47***, 324 (1980).
12. E. T. Cheng, et al., "Actinide Transmutation with Small Tokamak Fusion Reactors", *Proc. Int. Conf. Evaluation of Emerging Nuclear Fuel Cycle Systems*, Versailles, France (1995).
13. Y-K. M. Peng and E. T. Cheng, "Magnetic Fusion Driven Transmutation of Nuclear Waste (FTW)", *J. Fusion Energy, **12***, 381 (1993).
14. E. T. Cheng and R. J. Cerbone, "Prospect of Nuclear Waste Transmutation and Power Production in Fusion Reactors", *Fusion Technology, **30***, 1654 (1996).
15. Y. Gohar, "Fusion Option to Dispose of Spent Nuclear Fuel and Transuranic Elements", Argonne National Laboratory report ANL/TD/TM00-09 (2000).
16. L. J. Qiu, Y. C. Wu, B. J. Xiao, et al., "A Low Aspect Ratio Tokamak Transmutation System", *Nuclear Fusion, **40***, 629 (2000).
17. W. M. Stacey, "Capabilities of a DT Tokamak Fusion Neutron Source for Driving a Spent Nuclear Fuel Transmutation Reactor", *Nucl. Fusion, **41***, 135 (2001).
18. W. M. Stacey, J. Mandrekas, E. A. Hoffman, et al., "A Fusion Transmutation of Waste Reactor", *Fusion Sci. Technol., **41***, 116 (2002).
19. A. N. Mauer, W. M. Stacey, J. Mandrekas and E. A. Hoffman, "A Superconducting Fusion Transmutation of Waste Reactor", *Fusion Sci. Technol.,* **45**, 55 (2004).
20. J. Mandrekas, L. A. Cottrill, G. C. Hahn and W. M. Stacey, "An Advanced Tokamak Neutron Source for a Fusion Transmutation of Waste Reactor", Georgia Tech report GTFR-167 (2003).
21. W. M. Stacey, "Transmutation Missions for Tokamak Fusion Neutron Sources", *Fusion Engr. Des.*, to be published (2004).
22. W. M. Stacey, et al., "A Sub-Critical, Gas-Cooled Fast Transmutation Reactor (GCFTR) with a Fusion Neutron Source", *Nucl. Technol.*, submitted (2004).
23. E. A. Hoffman and W. M. Stacey, "Comparative Fuel Cycle Analysis of Critical and Subcritical Fast Reactor Transmutation Systems", *Nuclear Technol.*, **144**, 83 (2003).
24. E. A. Hoffman and W. M. Stacey, "Nuclear Design and Analysis of the Fusion Transmutation of Waste Reactor", *Fusion Sci. Technol.*, **45**, 51 (2004).
25. ITER website www.iter.org .
26. F. H. Southworth, et al., "The Next Generation Nuclear Plant (NGNP) Project", Proc. Global-3 Conf. (2003).
27. ATW Separatations Technologies and Waste Forms Technical Working Group, "A Roadmap for Developing ATW Technology: Separations and Waste Forms Technology", ANL-99/15, Argonne National Laboratory (1999).
28. B. J. Toppel, "A User's Guide to the REBUS-3 Fuel Cycle Analysis Capability", ANL-83-2, Argonne National Laboratory (1983).
29. B.B. Kadomtsev, B.N. Kolbasov, G.F. Churakov, A.S. Kukushkin, A.I. Kostenko, V.I. Pistunovich, S.N. Sadakov, G.E. Shatalov, D.V. Serebrennikov, USSR-Contribution to the Phase IIA of the INTOR Workshop, Vol 2, VIII-64 (1982).
30. ARIES web site aries/ucsd.edu/aries.
31. W. M. Stacey, "Tokamak Demonstration Reactors", *Nucl. Fusion,* **35**, 1369 (1995).

3. References for Transmutation Reactor Tokamak Neutron Source

1. "First Phase P&T Systems Study: Status and Assessment Report on Actinide and Fission Product Partitioning and Transmutation", OECD/NEA, Paris (1999).
2. "Proc. 1st-5th NEA International Exchange Meetings", OECD/NEA, Paris (1990,92,94,96,98).
3. "Nuclear Wastes--Technologies for Separations and Transmutations", National Research Council, National Academy Press, Washington (1996).
4. W. M. Stacey, J. Mandrekas, E. A. Hoffman, et al., "A Fusion Transmutation of Waste Reactor", *Fusion Sci. Technol.,* ***41***, 116 (2002).
5. W. M. Stacey, et al., "A Sub-Critical, Gas-Cooled Fast Transmutation Reactor (GCFTR) with a Fusion Neutron Source", *Nucl. Technol.*, submitted (2004).
6. E. A. Hoffman and W. M. Stacey, "Comparative Fuel Cycle Analysis of Critical and Subcritical Fast Reactor Transmutation Systems", *Nuclear Technol.*, **144**, 83 (2003).
7. W. M. Stacey, "Nuclear Reactor Physics", Wiley-Interscience, New York (2001), chapter 5.
8. W. M. Stacey, "Space-Time Nuclear Reactor Kinetics", Academic, New York (1969).
9. W. M. Stacey, "Temperature-Density Stability in Tokamak Reactors Operating on the DT Cycle", Nucl. Fusion, 15, 63 (1975).
10. J. Mandrekas and W. M. Stacey, "Evaluation of Different Control Methods for the International Thermonuclear Experimental Reactor", Fusion Technol., 19, 57 (1991).

C. WORK IN SUPPORT OF FIRE

1. Background

Over the duration of the Fusion Ignition Research Experiment (FIRE) study, the Georgia Tech Fusion Research Center performed physics simulations utilizing unique computational tools and analysis capabilities that have been built up over more than a decade of such work. These capabilities include: 1) a 1½-D plasma transport code with multiple impurity species and charge states, that has been used to develop the impurity-seeded radiative mantle power exhaust concept for ITER, in supporting analyses for the 2002 SNOWMASS workshop, and for FIRE; and 2) a global profile-averaged core power balance code that has been widely used for POPCON analysis of FIRE and in supporting analyses of other proposed Burning Plasma experiments for the SNOWMASS workshop.

2. FIRE Performance Evaluation Studies

We performed 0-D simulations using our profile-averaged tokamak power balance code to evaluate the performance of FIRE under various operating scenarios and to compare FIRE against other candidate burning physics experiments (BPX).

In Fig. 10, a POPCON plot for the reference FIRE design parameters is shown. The thick black line represents the boundary of the operating space which is defined by $Q > 5$, $P/P_{LH} > 1$, $P_{aux} < P_{aux}$ (max), $\beta_N < 2.0$ and $n/n_{Gr} < 1$, where P/P_{LH} is the ratio of the output power to the L-H threshold power, P_{aux}(max) is the maximum available auxiliary power for the device, β_N is the normalized beta and n/n_{Gr} is the Greenwald density limit fraction.

To explore the sensitivity of the operating space to the confinement scaling itself, POPCONs were constructed using various extensions of the IPB98(y,2) scaling. In Fig. 11, a POPCON for the FIRE reference assumptions is shown, using Cordey's extension of the IPB98(y,2) scaling (*J.G. Cordey, et al., 28th EPS Conf. on Contr. Fusion and Plasma Phys., 2001*) which attempts to account for the effects of triangularity, proximity to the Greenwald density limit and density peaking.

The results of our FIRE performance evaluation studies have been published in various project reports and presented at international meetings[1-3].

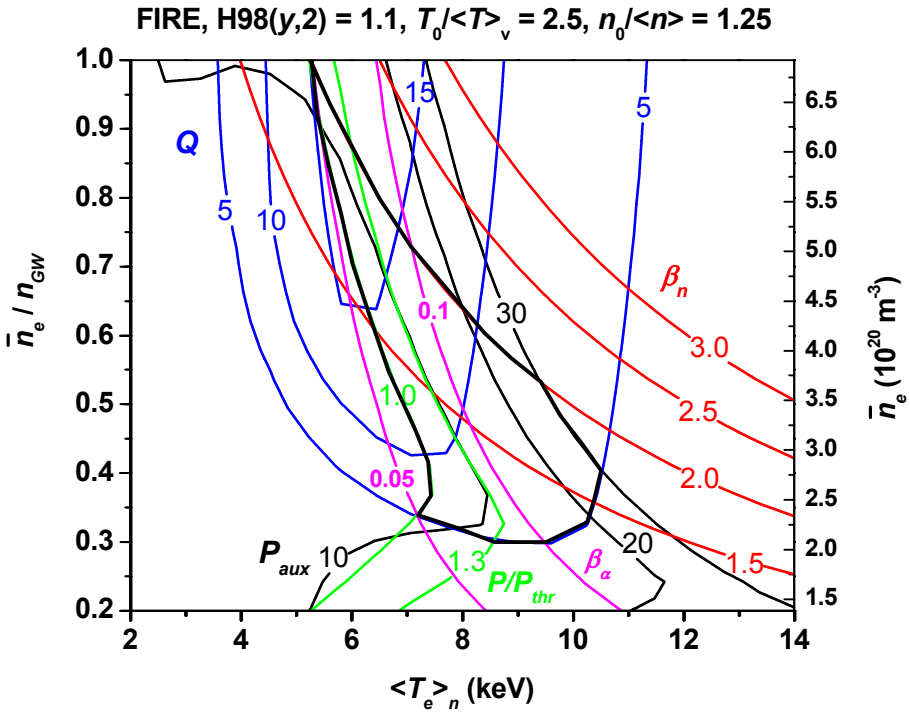

Figure 10: FIRE POPCON for the reference design assumptions.

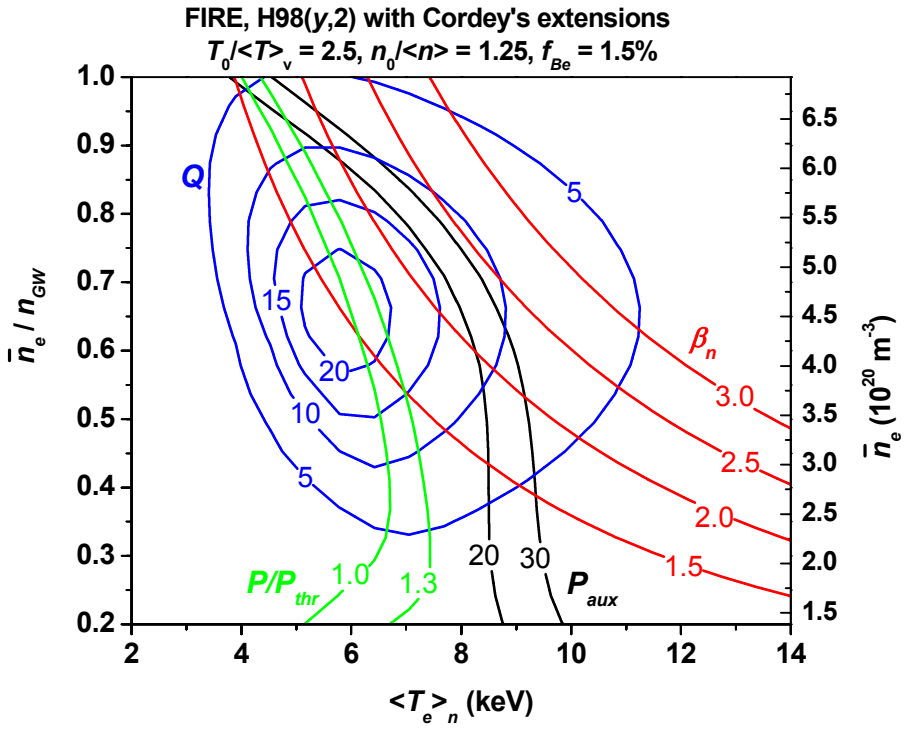

Figure 11: FIRE POPCON using the IPB98(y,2) scaling with Cordey's extensions.

3. 1½-D Transport Simulations

While 0-D simulations provide us with a valuable insight into the operating space of each reactor design and its sensitivity to several uncertain parameters, time-dependent simulations of the reference operating scenario with 1½-D transport codes employing theory-based transport models are still necessary to assess the performance projections of FIRE and other BPXs. We performed such simulations for the FIRE reference operating scenario with our GTWHIST 1½-D transport code[4] and using the latest version of the GLF23 transport model. In Fig. 12, the time histories of various power balance quantities are shown. We found that the performance of the reactor was very sensitive to the pedestal temperature. A pedestal temperature of about 4 keV was required to achieve $Q = 10$ at a Greenwald density limit fraction of 0.75.

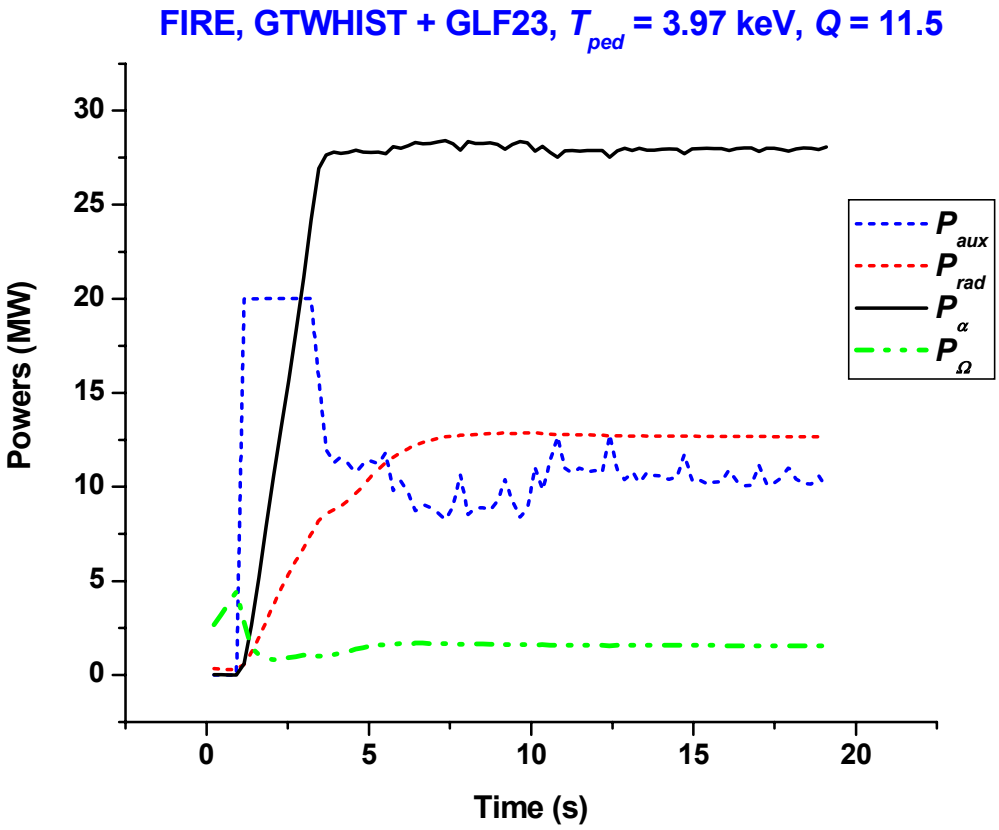

Figure 12: Time history of various power balance parameters of the FIRE reference scenario using the GLF23 transport model.

4. Impurity Transport Simulations for FIRE

We performed transport simulations with our 1½-D main plasma – multi charge state impurity transport code GTWHIST, in order to evaluate the impact of impurity seeded operation on the performance of FIRE.

While the new FIRE divertor design[5] can withstand the anticipated heat loads from the plasma core during the standard ELMy H-mode operation of the device, enhanced radiation from seeded impurities from the plasma mantle and the divertor is expected to be necessary during the higher power Advanced Tokamak (AT) operating mode in order to maintain a flexible operating space.

As a first step, the entire* FIRE reference operating scenario was modeled with GTWHIST and compared to the reference TSC simulation[6]. The results of this benchmarking simulation are shown in Fig. 13, where time histories of various global power quantities are plotted. A fixed-shape transport model normalized to yield an H-factor of about 1 relative to the ITER IPB(y,2) global confinement scaling was adopted for these simulations.

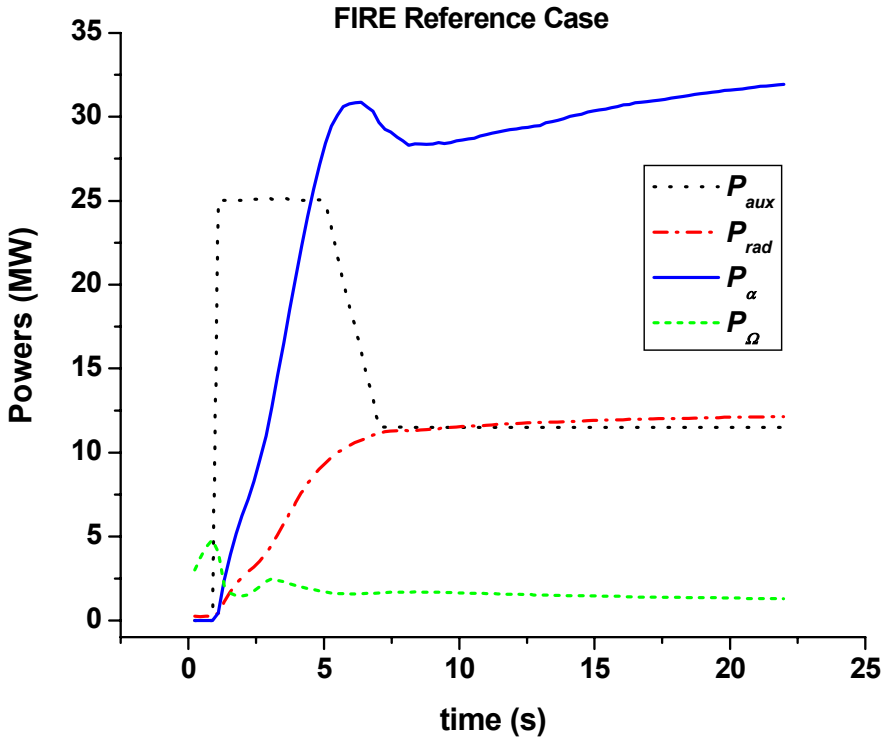

Figure 13: GTWHIST evaluation of the time history of various global power balance parameters for the FIRE reference case.

Following the establishment of the reference discharge, Argon impurities were injected at the edge of the device and their evolution and contribution to the power balance were followed using the multi-charge state impurity transport capabilities of the GTWHIST code. A fixed diffusion coefficient of 0.5 m^2/s for all impurity charge states and no inward pinch have been assumed in these simulations. The profiles of the various Ar charge states are shown in Fig. 14, for a 0.3% global Ar concentration.

* Since the MHD part of the GTWHIST code supports fixed-boundary configurations only, our simulation starts when the plasma geometry and fields (major and minor radii and toroidal magnetic field) are at their reference values, corresponding to about 4 seconds in the TSC simulation.

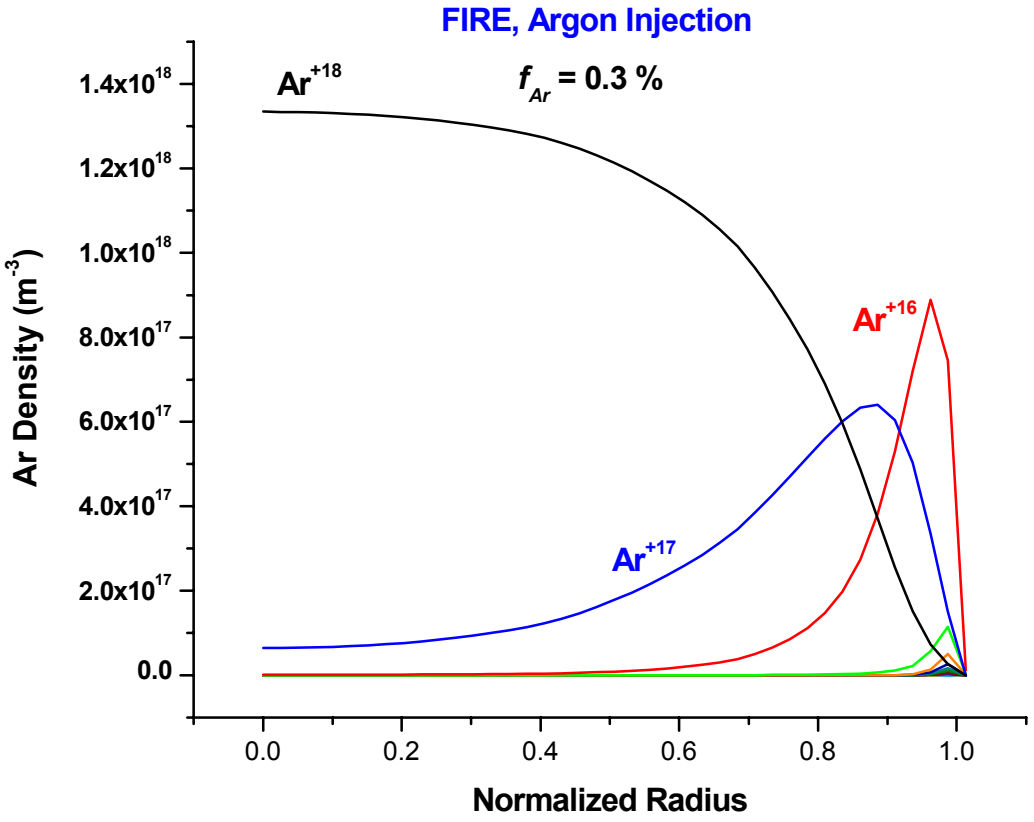

Figure 14: Profiles of Argon charge states following Ar injection.

As expected, Ar is almost fully ionized in the plasma core, while the highly radiating Lithium-like and Helium-like charge states are concentrated in the plasma edge. Our simulation predicts that for the reference concentration of 0.3%, the total radiated power by the Ar impurities (including bremsstrahlung and line radiation) is 45.2 MW, which is about 20%-30% higher than the predictions of earlier 0-D (fixed profiles) simulations. This suggests that lower Ar concentrations may be adequate to meet the needs of the FIRE design.

In addition to the determination of the radiating properties of the seeded Ar impurities, our simulations identified a number of critical issues that must be addressed before impurity seeding can be safely adopted as part of the reference operating scenario of FIRE. These include: a) the potential of edge thermal instabilities following Ar injection which were observed in several of our simulations and which can collapse the edge temperature profile and, eventually, terminate the plasma; b) the sensitivity of our predictions to the edge temperature assumptions, underlying the need for a realistic and accurate pedestal boundary condition model; c) the

importance of the edge ion and electron thermal transport assumptions; and d) the possibility of core impurity accumulation due to neoclassical effects arising from peaked density profiles.

5. References for FIRE work

1. D.M. Meade, S.C. Jardin, J.A. Schmidt, R.J. Thome , N.R. Sauthoff , P. Heitzenroeder, B.E. Nelson, M.A. Ulrickson, C.E. Kessel , J. Mandrekas, C.L. Neumeyer , J.H. Schultz , P.H. Rutherford, J.C. Wesley , K.M. Young, W.M. Nevins, W.A. Houlberg , N.A. Uckan, R. W. Woolley & C. C. Baker, "Mission and Design of the Fusion Ignition Research Experiment (FIRE)," IAEA-CN-77/FTP2/16, presented at the 18th IAEA Fusion Energy Conference, Sorrento, Italy, Oct. 4-10, 2000.
2. D.M. Meade, C.E. Kessel, G.W. Hammett, S.C. Jardin, M.A. Ulrickson, P. Titus, P. Heitzenroeder, B.E. Nelson, J.H. Schultz, R.J, Thome, J.C. Wesley, J. Mandrekas, G.A. Navratil, J. Bialek, T. Rognlien, T.K. Mau, R. Budny, N. Gorelenkov, P.H. Rutherford, K.M. Young, and J.A. Schmidt, "Exploration of Burning Plasmas in FIRE", IAEA-CN-94/FT2-6, presented at the 19th IAEA Fusion Energy Conference, Lyon, France, 14-19 October, 2002.
3. D. M. Meade, N. R. Sauthoff, C. E. Kessel, S. C. Jardin, G.A. Navratil, J. Bialek, M. A. Ulrickson, T. Rognlein, J. Mandrekas, C. K. Skinner, G. Hammett, R.V. Budny, G. Kramer, N. Gorelenkov, T K. Mau, P. H. Rutherford, K. M. Young, D. W. Swain, P Bonoli, J. Decker and J. A. Schmidt, "High-β Steady-State Advanced Tokamak Regimes for ITER and FIRE," to be presented at the 20th IAEA Fusion Energy Conference, November 2004.
4. J. Mandrekas, W. M. Stacey, F. A. Kelly, "Impurity Seeded Radiative Power Exhaust Solutions for ITER", *Nucl. Fusion*, **36**, 917 (1996).
5. M. Ulrickson, et al., "Issues and Recent Advances on PFCs for ITER and FIRE", Bull. Am. Phys. Soc., **48** 343 (2003).
6. C. Kessel, PPPL, personal communication, Dec. 2003.

D. NTCC PARTICIPATION

1. Introduction

The Georgia Tech Fusion Research Center has been participating in the National Transport Code Collaboration (NTCC) project since 1999. During this period, we have reviewed several submitted modules and have submitted two modules of our own.

2. Submitted Modules

NBEAMS module (submitted in 1999)

We have submitted the module NBEAMS, which contains routines for the calculation of neutral beam heating and current drive parameters in tokamak plasmas. It calculates the NB deposition profile, profiles of the NB heating power deposited to the background ions and electrons, various NB current drive quantities and, optionally, several beam-target fusion quantities.

The NBEAMS module was originally developed by the author for the ITER systems code SUPERCODE[1] and it was used extensively during the ITER CDA and EDA design activities. The

calculation is approximate (it is based on the diffuse beam approximation and it assumes a simplified flux surface geometry) but computationally fast. Extensive benchmarks with more detailed codes (ACCOME, NFREYA, TRANSP) have consistently shown excellent agreement

Before submission to the NTCC library, the module was updated, tested and extensively modified to conform to the NTCC standards. The module is intended to be used in transport simulations where a realistic NB heating profile is desired, but the full accuracy of more detailed (and computationally expensive) codes such as the NUBEAM Monte Carlo fast ion package (also submitted to NTCC) is not necessary.

GTNEUT module (submitted in 2004)

We recently submitted the GTNEUT module. This module contains our 2-D neutral transport code GTNEUT[2] which is based on the Transmission & Escape Probability (TEP) method[3]. While other neutral modules have been submitted to NTCC (NUT, FRANTIC), the computational speed of GTNEUT and its ability to handle complex geometries, like the ones encountered at the edge of tokamak plasmas, make it an ideal tool for edge plasma and core fueling simulations. The code has been extensively benchmarked against Monte Carlo and experiment[4-6].

3. Reviewed Modules

We have reviewed five NTCC modules and are in the process of reviewing a sixth. Each review usually consists of ensuring that the module conforms to the NTCC standards, followed by building, testing and installing the module on various computer platforms (usually workstations running different versions of the UNIX operating system). In addition to the test programs supplied by the module developers, we often write our own testing routines to exercise the capabilities of the module and to test various usability and implementation issues. During the review process, we communicate with the module developers to resolve any problems which we identified, and offering suggestions for improvements. Following each review, a standardized evaluation form is filled out and submitted to the NTCC Committee chairman with our comments and recommendation, and then the module is put to a vote by the chairman for the NTCC committee members.

We have reviewed the following modules, which are now accepted as part of the NTCC module library:

FPREPROC (reviewed and approved in 2000)

The Fortran Pre-processor module *FpreProc* (submitted by Doug McCune of PPPL) is a set of PERL scripts that pre-process Fortran (f77 and f90) code using GNU's *gcc* compiler. It provides a simple and elegant code pre-processing mechanism for specifying conditional compilation and/or compile time macro expansion, greatly aiding the ability to maintain from a single source a code which compiles and runs correctly on many types of target architectures. The advantage of *FpreProc* over comparable tools such as *fpp* is that it should work the same on all systems (vendor-supplied Fortran preprocessors can be system and architecture dependent).

PORTLIB (reviewed and approved in 2000)

The *PortLib* portability tools library (submitted by Doug McCune of PPPL) contains a number of useful routines and functions that perform certain system tasks. Some of these tasks are very common (e.g. elapsed CPU time, access to command line arguments, access to the shell, etc.) and can be found in almost every code. While most Fortran compilers provide access to such routines, the interface is not standard forcing the developer to re-write part of his/her code and use conditional compilation every time the code is ported into a new environment The *PortLib* library provides a standardized interface to these routines, greatly simplifying the porting of codes to new platforms.

XPLASMA (reviewed and approved in 2002)

The XPLASMA module (submitted by Doug McCune of PPPL) is a set of routines that provides a representation standard for MHD equilibria in axisymmetric plasmas using spline interpolation. The biggest advantage of XPLASMA is the elimination of the need that physics modules share the same MHD representation and grids as the main transport code. This makes it easier to port physics modules into transport codes, since one does not have to write interface code (a non-trivial task usually) to translate from one representation to another (e.g. from an inverse equilibrium representation to an *R,Z* representation and vice versa). In addition, the XPLASMA module is an integral part of the Monte Carlo fast ion code NUBEAM which has also been submitted to NTCC.

NUT (reviewed and approved in 2003)

NUT (submitted by P.M. Valanju, University of Texas). NUT is a fast, semi-analytic algorithm for 3-D neutral transport in 3-D plasmas and can be a useful module for calculating fueling of fusion reactors.

LSC module

The Lower Hybrid Simulation Code module **LSC** (developed by David Ignat and submitted by Doug McCune, PPPL), has been submitted to NTCC and is considered a high priority module, since there is a need for plasma heating source modules.

Our work with the LSC module has been more than a typical NTCC review, since the current version of the module is not up the NTCC standards. Besides coding and portability issues–which are not that hard to rectify–the module is missing a number of potentially significant physics effects, the most important of which is the absence of trapped electron effects.

We have a developed a routine to calculate trapped electron effects for LH current drive based on the work by Ron Cohen[7]. Additionally, a trapped electron correction routine from the ACCOME code based on the adjoint technique and developed by Karney and Fisch has been provided to us by Paul Bonoli from MIT. The revised LSC code will be re-submitted to NTCC after benchmarking with other codes such as the ACCOME code have been completed.

CYTRAN (reviewed in 2004, pending final approval by the NTCC committee)

The **CYTRAN** module (submitted by Wayne A. Houlberg, ORNL) calculates the radial profile of synchrotron/cyclotron radiation loss (or gain) for toroidal plasmas. While cyclotron radiation is rather small in present-day experiments—at least compared to bremsstrahlung and impurity radiation—and is usually neglected in most numerical simulations, its strong dependence on plasma temperature and magnetic field strength will increase its importance in next-generation burning plasma experiments. Cyclotron radiation exhibits strong non-local effects where the wall-reflected radiation is often reabsorbed in the plasma edge giving rise, in effect, to a local *heating* rather than *cooling* term in the outer plasma. This means that the commonly used approach in a number of radial transport codes of taking a global formula for the cyclotron radiation loss (e.g., Trubnikov's expression) and applying it locally is questionable at best. A true radial transport approach is needed to accurately account for the radial profile of the cyclotron radiation cooling or heating rate. CYTRAN is such a routine and has been used in the WHIST code and its derivatives for a couple of decades.

FRANTIC (under review)

The FRANTIC module (submitted by Doug McCune of PPPL) calculates neutral particle transport in cylindrical plasmas based on the semi-analytic technique by S. Tamor[8]. This module is currently under review.

4. NTCC References

1. S.W. Haney, et al., *Fusion Technol*. **21** (1992) 1749.
2. J. Mandrekas, *Comp. Phys. Commun*. **161** (2004) 36.
3. W.M. Stacey and J. Mandrekas, *Nucl. Fusion* **34** (1994) 1385.
4. W. M. Stacey, J. Mandrekas and R. Rubilar, *Fusion Sci. Technol*. **40** (2001) 66.
5. R. Rubilar, W. M. Stacey and J. Mandrekas, *Nucl. Fusion* **41** (2001) 1003.
6. J. Mandrekas, R. J. Colchin, W. M. Stacey, et al., *Nucl. Fusion* **43** (2003) 314.
7. R.H. Cohen, *Phys. Fluids* **30**, (2442) 1987.
8. S. Tamor, J. Comput. Phys. 40 (1981) 104.